Ore Geology Reviews 104 (2019) 722–744

Contents lists available at ScienceDirect

Ore Geology Reviews

journal homepage: www.elsevier.com/locate/oregeorev

Platinum-group element geochemistry of boninite-derived Mesoarchean chromitites and ultramafic-mafic cumulate rocks from the Sukinda Massif (Orissa, India)

Sisir K. Mondal[a,*], Sarifa Khatun[b,1], Hazel M. Prichard[c,2], M. Satyanarayanan[d], G.R. Ravindra Kumar[e]

[a] Department of Geological Sciences, Jadavpur University, 188, Raja S.C. Mullik Road, Kolkata, WB 700032, India
[b] Department of Geology, Jogamaya Devi College, Kolkata WB-700026, India
[c] School of Earth and Ocean Sciences, Cardiff University, Cardiff CF10 3AT, UK
[d] CSIR-National Geophysical Research Institute, Hyderabad, Telangana 500007, India
[e] MoES-National Centre for Earth Science Studies, Akkulam, Trivandrum 695011, India

ARTICLE INFO

Keywords:
Chromitite
Platinum-group elements (PGE)
Platinum-group mineral (PGM)
Os-Ir-Ru alloys
Boninite
Sukinda Massif

ABSTRACT

The Mesoarchean Sukinda Massif in the Singhbhum craton is the largest chromite ore deposit in India that contains ≈95% of Indian Cr resources. The Sukinda Massif consists of an elongated layered ultramafic unit (≈25 km × 400 m) that occurs within the 3.5 Ga supracrustal sequences of the Tomka-Daitari-Mahagiri greenstone belt in eastern India. The ultramafic unit comprises serpentinized dunite, orthopyroxenite and chromitite. There are six chromitite seams which are present within the serpentinized dunite. All ultramafic rocks are extensively weathered and capped by laterites (≈30 m thick). In the southwestern part of the Sukinda Massif, in the Katpal area, chromitite seams and the host ultramafic rocks are fragmented, forming breccias cemented by the gabbroic to granodioritic rocks. Whole-rock major, trace and platinum-group elements (PGE) geochemistry indicates that the ultramafic unit and the gabbro, including the cementing matrix materials of the breccias, are cogenetic. The ultramafic rocks formed by fractional crystallization of a parental boninitic or high-Mg siliceous magma. The cementing gabbroic rocks formed from an evolved boninitic magma generated from fractionated boninite or high-Mg siliceous basalt. The positive correlation between MgO and Ni, and MgO and Cr is due to fractionation of early cumulus like olivine and chromite from the high-Mg parental magma. The correlation between Zr and Cu suggests that the parental boninitic magma was S-undersaturated. However, the matrix gabbro shows a flatter trend with increasing Zr and Cu, indicating sulfide saturation occurred later in the evolved boninitic magma. In Sukinda, the concentrations of PGE in the massive chromitites (≈176–875 ppb) from the main ultramafic unit and in chromitite fragments (≈61–279 ppb) from the breccias are higher than in serpentinite (≈19–71 ppb), orthopyroxenite (≈14–19 ppb) and gabbro (≈3–11 ppb). Three samples of the massive chromitites from the main ultramafic unit have significant PGE concentrations (PGE_{total} ≈ 651–875 ppb) with IPGE (Ir, Os, Ru) ≈ 528–634 ppb, much higher than PPGE (Pd, Pt, Rh) ≈ 93–332 ppb. Detailed PGE mineralogical studies of these samples revealed presence of IPGE-bearing platinum-group minerals (PGM) dominated by Os-Ir-Ru alloys (containing minor Pt) enclosed in chromite grains. Other PGMs are laurite present as composite grain within chromite plus irarsite which are associated with cracks in chromite grains and a small sperrylite grain attached to an Os-Ir-Ru alloy. All the As-bearing PGM are associated with cracks in the chromite suggesting introduction of As during alteration of primary PGM to PGM-arsenides. The positive correlation between IPGE (Os, Ir, Ru) and MgO or Cr indicates they are fractionated during the early stage of magmatic differentiation from a S-undersaturated boninitic magma. The low Ir of the silicate rocks indicate prior removal of Ir-bearing alloys from the parental boninitic magma which would account for the occurrence of Os-Ir-Ru alloys in massive chromitites. The results suggest that Os-Ir-Ru alloys from the Sukinda chromitites crystallized at relatively high temperature and low fS_2 condition within a S-undersaturated boninitic magma ascending from the upper mantle where they entrapped by the growing chromite crystals.

* Corresponding author.
E-mail address: sisir.mondal@gmail.com (S.K. Mondal).
[1] Current address: Department of Geology, Presidency University, Kolkata, WB 700073, India.
[2] Deceased, Jan 1, 2017.

https://doi.org/10.1016/j.oregeorev.2018.11.027
Received 7 May 2018; Received in revised form 28 October 2018; Accepted 28 November 2018
Available online 30 November 2018

Overall, the initial PGE analysis from the Sukinda breccias, presented herein, indicate similarities with the Nuasahi breccias in the Singhbhum craton, and highlight the potential for mineralization in this area.

1. Introduction

Chromite deposits are recorded from early Archean to Phanerozoic: among these the early to Mesoarchean (≈3400–3100 Ma) chromite deposits are in general associated with sill-like ultramafic bodies within some greenstone belts (e.g., Stowe, 1994; Mondal et al., 2006; Mondal, 2009; Mukherjee and Mondal, 2018). Common examples include the chromite deposits in the Archean Shurugwi greenstone belt of the Zimbabwe craton in Southern Africa and within the Archean greenstone belts of the Indian Shield (Fig. 1a). These layered sill-like ultramafic bodies are conformably present within the volcano-sedimentary rocks of the Archean greenstone sequences and considered to be genetically linked with the siliceous high-Mg basaltic or boninitic and low-Al komatiitic magmas (e.g., Mondal et al., 2001, 2006; Mukherjee et al.,

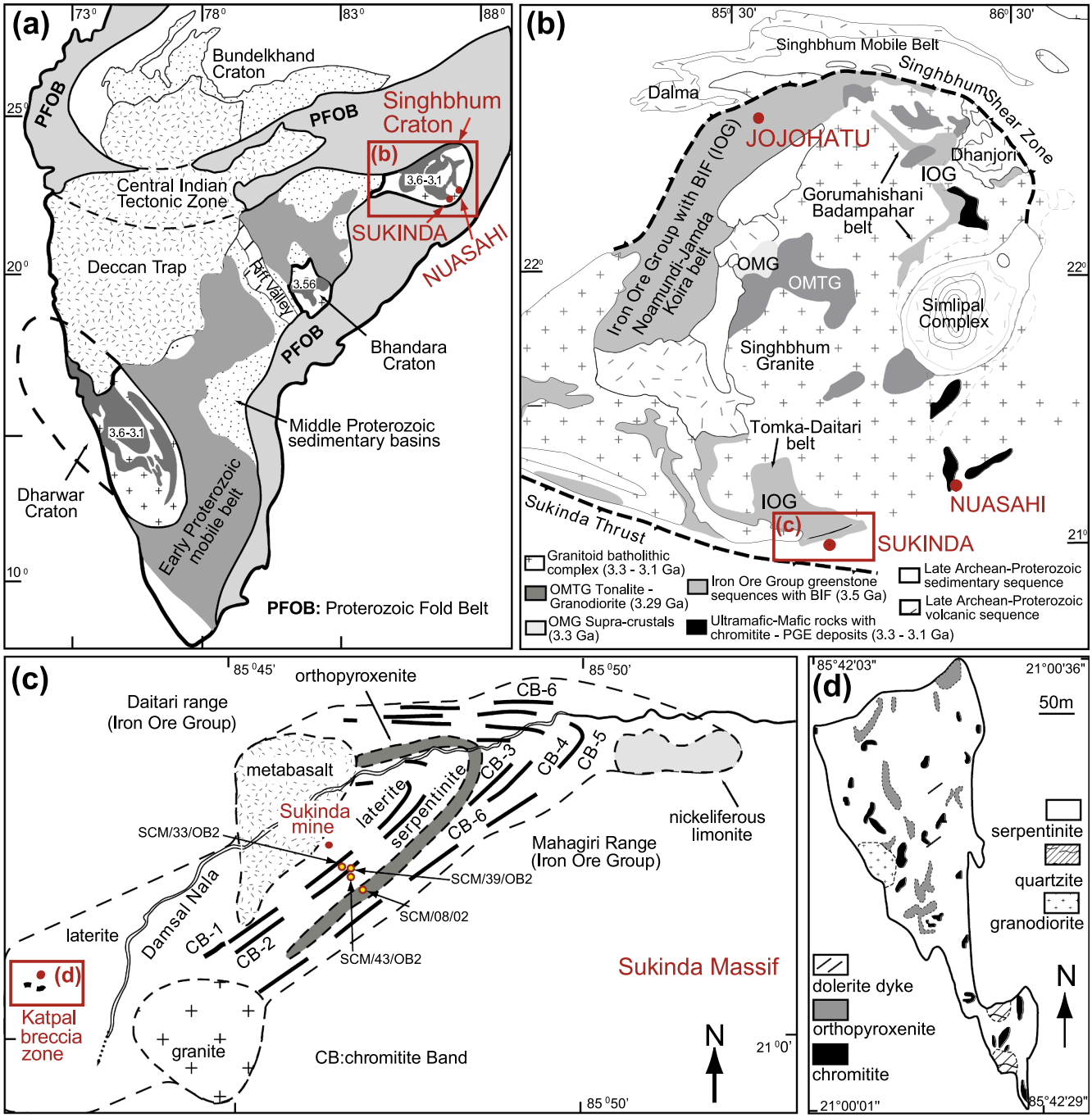

Fig. 1. (a) General geology of the Indian Shield showing the four Archean cratons (after Radhakrishna and Naqvi, 1986; Leelananadam et al., 2006). (b) Geology of the Singhbhum craton, India (after Saha, 1994; Mondal et al., 2006). (c) Geology of the Sukinda Massif (after Basu et al., 1997). (d) Geology of the Katpal area (after Sen and Mohanty, 2005).

2010, 2015). The chromite-bearing ultramafic bodies within the greenstone belts are in general serpentinized, extensively sheared and deformed. The chromite-bearing ultramafic bodies of the Nuasahi-Sukinda-Jojohatu igneous complexes in the Singhbhum craton (eastern India) and the Nuggihalli–Krishnarajpet–Holenarsipur–Nagamangala-Javanhalli igneous complexes in the Western Dharwar craton (southern India) are the common examples of similar sill-like ultramafic bodies within the Indian Archean greenstone belts (Mondal et al., 2006, 2007; Mondal, 2009; Mondal and Zhou, 2010; Khatun et al., 2014; Mukherjee et al., 2012, 2014; Majumdar et al., 2016a,b). Among these occurrences, the Sukinda Massif (≈25 km long) in Jajpur district of the Orissa state from eastern India contains > 95% of India's chromium ore resources (e.g., Mondal et al., 2006).

The chromite deposits of the Sukinda Massif are present within the Sukinda valley at the southern part of the Singhbhum craton (Fig. 1b and c). The chromitite ore bodies in the Sukinda Massif occur as persistent layers or as lenses and pockets within the serpentinized and silicified dunite-peridotite rocks (e.g., Banerjee, 1972). Previous works on the Sukinda Massif mainly concentrated on the chromite mineralization of the main ultramafic unit (e.g., Chakraborty and Baidya, 1978; Chakraborty and Chakraborty, 1984; Pal and Mitra, 2004; Mondal et al., 2006). Based on some limited platinum-group element (PGE) data from the chromitites, Page et al. (1985) characterized the Sukinda Massif as part of an Archean ophiolitic complex. Acharyya (1993) suggested possibilities of the chromite-bearing ultramafic cumulates of the Sukinda (and Nuasahi) Massifs being part of the conformable and tectonically overlying Archean greenstone sequence, where complete and composite package could be compared with the present-day oceanic crust. Based on parental magma calculation from primary chromite compositions and tectonic discrimination diagrams Mondal et al. (2006) suggested that a boninitic (or low-Ti high-Mg siliceous basaltic) magma produced the ultramafic rocks including the chromitites of the Sukinda, and in a supra-subduction zone setting in the Archean.

Detail work on the geochemical variations in terms of major, trace and platinum-group elements (PGE) of the massive chromitites and the host ultramafic cumulate rocks of the Sukinda Massif has not been previously undertaken. In this study, we report extensive whole-rock major, trace and platinum-group element data for chromitite, serpentinite, orthopyroxenite and breccia assemblage rocks from the Sukinda Massif. In addition, we report the detailed PGE-mineralogy of some selected chromitite samples from the chromitite ore bodies, which we have found containing significant values of PGEs. The main aim of this research is to investigate on the PGE prospect of the Sukinda Massif using bulk rock geochemistry and to characterize the platinum-group minerals (PGM) in the chromitites. The additional goals of this paper are to understand the processes responsible for PGE fractionation during differentiation of the parental magmas, and the origin of the diversity of PGE concentrations in different rock units of the Sukinda Massif.

2. Geological background

The chromite deposits of the Sukinda Massif are located in the southwestern part of the Singhbhum craton (Fig. 1b). The Singhbhum craton is bounded by the Singhbhum shear zone to the north and by the Sukinda thrust to the south. There are several granitoid batholiths in the Singhbhum craton; the Singhbhum Granite Complex is the largest batholithic complex (3.3–3.1 Ga; Mishra et al., 1999). Among the supracrustal rocks within the Singhbhum craton, the amphibolite-facies metaigneous and metasedimentary rocks comprise the Older Metamorphic Group (OMG; 3.3 Ga magmatic crystallization age, Sharma et al., 1994; 3.55 Ga zircon age, Mishra et al., 1999). The other supracrustal rock sequence in the Singhbhum craton is known as the Iron Ore Group (IOG; 3.5 Ga zircon age; Mukhopadhyay et al., 2008) that comprises the three major Archean greenstone belts within the Singhbhum craton: Jamda-Koira-Noamundi, Gorumahshani-Badampahar and Tomka-Daitari greenstone belts (Fig. 1b). These Archean greenstone belts contain sill-like layered ultramafic bodies with chromite ores, which are mainly present in the Nuasahi, Sukinda and Jojohatu areas (Mondal, 2008, 2009; Fig. 1b). In many places the chromiferous ultramafic bodies are closely associated with large gabbro unit containing Ti-V-bearing magnetitite bands e.g. in the Nuasahi area (Mondal and Baidya, 1996; Mondal and Zhou, 2010; Khatun et al., 2014; Prichard et al., 2017a). However, other than minor occurrence in the Katpal area, there is no such large gabbro unit so far reported from the Sukinda Massif (Fig. 1c and d).

The chromite deposits of the Nuasahi Massif are located at the eastern part of the Sukinda Massif and also hosted within the metasedimentary and metaigneous rocks of the IOG (Fig. 1b). The ultramafic bodies of the Nuasahi Massif consist of sub-vertical dunite and orthopyroxenite with minor harzburgite. Three major chromitite ore bodies are hosted within the serpentinized dunite (Fig. 1b). In the Nuasahi Massif a tectonic breccia zone is present at the upper contact of the ultramafic unit with the gabbro (Mondal and Baidya, 1997; Mondal et al., 2001). Fragments of lower ultramafic rocks and chromitites are present in the breccia zone, which are cemented by the pegmatitic gabbro. The breccia and the matrix pegmatitic gabbroic rocks contain base metal sulfides as veins, stringers and disseminations with highly anomalous PGE concentrations (up to 26 ppm; Mondal and Zhou, 2010; Khatun et al., 2014). The zircon U-Pb ages of the gabbroic matrix of the Nuasahi breccia are 3123 ± 7 and 3119 ± 6 Ma (Augé et al., 2003). The absolute ages of the ultramafic bodies of the Nuasahi and Sukinda Massifs have not yet been determined. Based on the Re-Os isotopic systematics of unaltered chromite from massive chromitites, Mondal et al. (2007) calculated a model mantle extraction age of around 3.5 Ga for the chromite-bearing ultramafic unit of the Sukinda and Nuasahi Massifs. However, based on field relationships and available Sm-Nd isochron ages for the associated gabbro (3.2 Ga; Augé et al., 2003), Mondal et al. (2006) have suggested that the Nuasahi and Sukinda Massifs were possibly formed between 3.3 and 3.1 Ga.

The occurrence of chromite deposits in the Sukinda valley was first reported in 1949 by the prospecting division of the Tata Iron and Steel Company (TISCO). The NE-SW trending sill-like layered ultramafic body of the Sukinda Massif occurs within the metasedimentary and metavolcanic rocks of the early Archean Tomka-Daitari greenstone belt (Fig. 1b and c). The intrusive ultramafic unit with chromitite ore bodies occurs as a SW-plunging synformal body within folded sequences of the greenstone belt (Banerjee, 1972). Two horizons of metabasalts are present; one at the base of the ultramafic unit in the east, and another at the synformal core in the west (Basu et al., 1997). The major rocks of the ultramafic unit are serpentinite (after dunite), orthopyroxenite and chromitite. The chromitite ore bodies occur over 25 km as discontinuous layers or as lenses and pockets within the serpentinized dunite. At least six deformed bands of chromitites are present (Fig. 1c; '**CB-1**' to '**CB-6**'). The chromitite ore bodies range in length from 200 m to 7 km and are ≈4–6 m thick (Mondal et al., 2006). The ultramafic rocks are commonly serpentinised or altered to talc-schist and talc-tremolite-schist and are weathered and lateritized to a depth of ≈30 m (e.g. Som and Joshi, 2002).

In the Katpal area, southwestern part of the Sukinda Massif (Fig. 1c and d), the ultramafic-hosted chromitite bodies are extensively fragmented, forming a tectonic breccia (Khatun et al., 2009). The breccias are impregnated by gabbroic to granodioritic melts that form the breccia matrix. The Katpal breccia is geologically similar to that found in the Nuasahi Massif, documented by Mondal and co-workers (Mondal, 2000; Mondal and Baidya, 1997; Mondal et al., 2001, 2006; Mondal and Zhou, 2010) however those from the Nuasahi area have notably higher sulfide and PGE abundances. Sarkar et al. (2001, 2003) described the occurrence of this breccia in the Katpal 'F' quarry of Orissa Mining Corporation (OMC) and reported occurrence of platinum-group minerals (PGM) in the chromitite breccia.

3. Petrography

3.1. Samples

Samples were collected systematically across strike, including different rock units and the chromitite ore bodies of the main ultramafic unit (Fig. 1c). Samples of the breccia were collected from the Katpal area along with chromitite, orthopyroxenite and gabbro (Fig. 1d). Some breccia samples were also collected from stockpiles of abandoned quarries. The sample details are provided in Annexure-A (available online). All samples were prepared as polished thin sections for petrographic study.

3.2. Main ultramafic unit

The ultramafic unit consists of serpentinized dunite, orthopyroxenite and chromitite (Figs. 1–3). The dunite is light green with disseminated black chromite grains (< 1 vol%). The rock is extensively serpentinized, commonly silicified, and often bearing talc, serpentine and chlorite. Coarse-grained orthopyroxenite is relatively unaltered and has accessory interstitial euhedral to subhedral chromite (< 1 vol%, Fig. 3b). In the Katpal area, the orthopyroxenite is more altered, and in some instances, orthopyroxene has been completely replaced by amphibole, talc and chlorite. Chromitite textures range from massive to schlieren-banded (Fig. 2a) and spotted where white spots are now represented by serpentine minerals after olivine (Fig. 2e). Chromite grains in the massive chromitites are commonly subhedral to euhedral in shape (Fig. 3a). In the interstitial spaces of chromites, serpentine (5–10 vol%), chlorite, and minor amount of base metal sulfide minerals are present.

3.3. Katpal chromitite-gabbro-breccia assemblage

In the Katpal area of the Sukinda Massif the chromitites and the host serpentinites of the main ultramafic unit are present as randomly oriented fragments/clasts of different shapes within coarse-grained

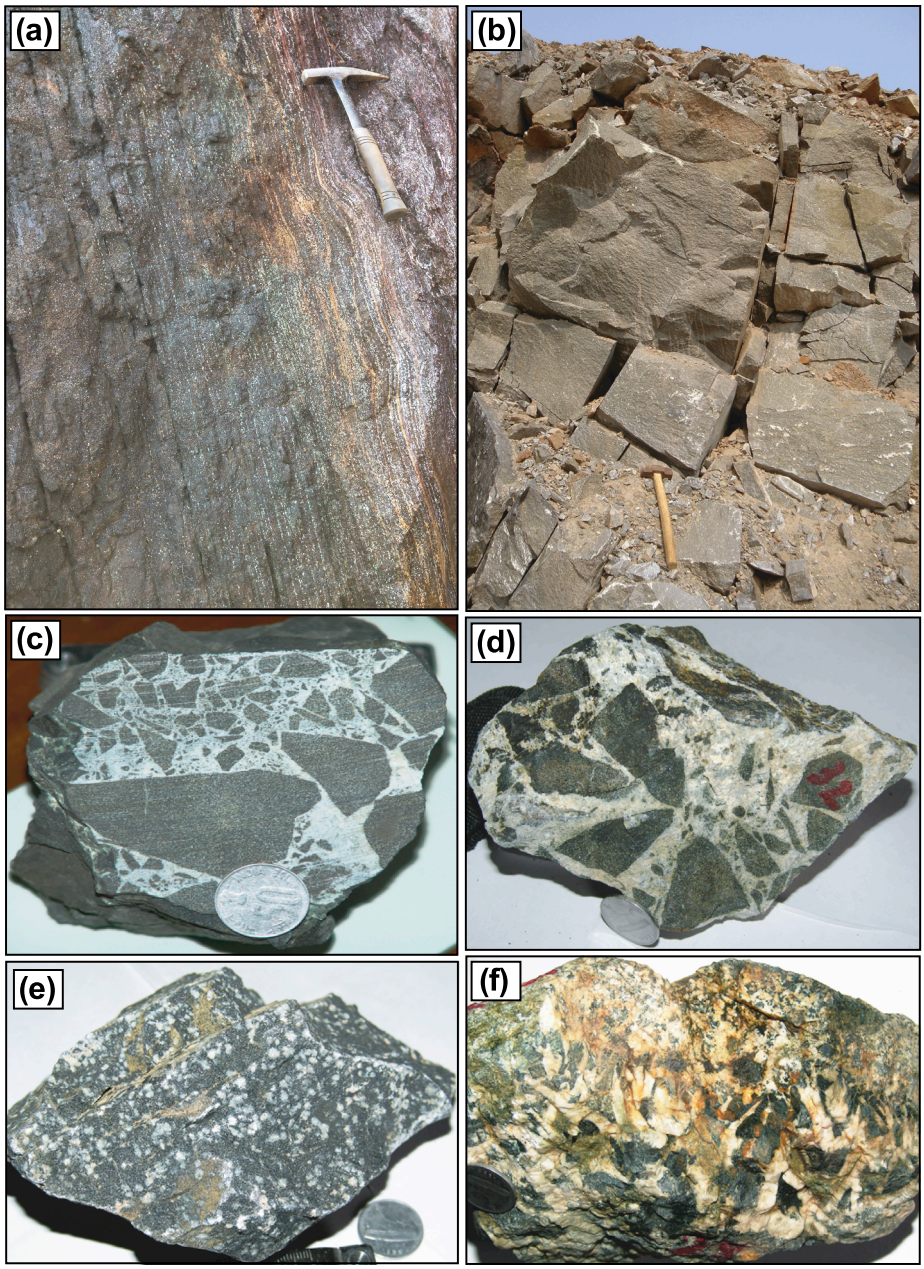

Fig. 2. Field photographs of (a) chromitite seam #1 (South Kaliapani mine, OMC) showing massive and schleiren banded chromitites, and (b) orthopyroxenite (Sukinda mine, TISCO). Photographs of the hand specimens: (c) Chromitite breccia where massive chromitite clasts of different sizes and shapes are present within altered gabbroic matrix; Sample no. KTPL-27, Katpal area; (d) Chromitite breccia where triangular chromitite clasts are pointing towards a centre; Sample no. KTPL-52, Katpal area; (e) Spotted chromitite; Sample no. KTPL-29, Katpal area; (f) Pegmatitic gabbro from Katpal area; plagioclase and pyroxene are present forming intergranular texture. Rock is medium to fine grained at the upper part. Sample no. KTPL-28.

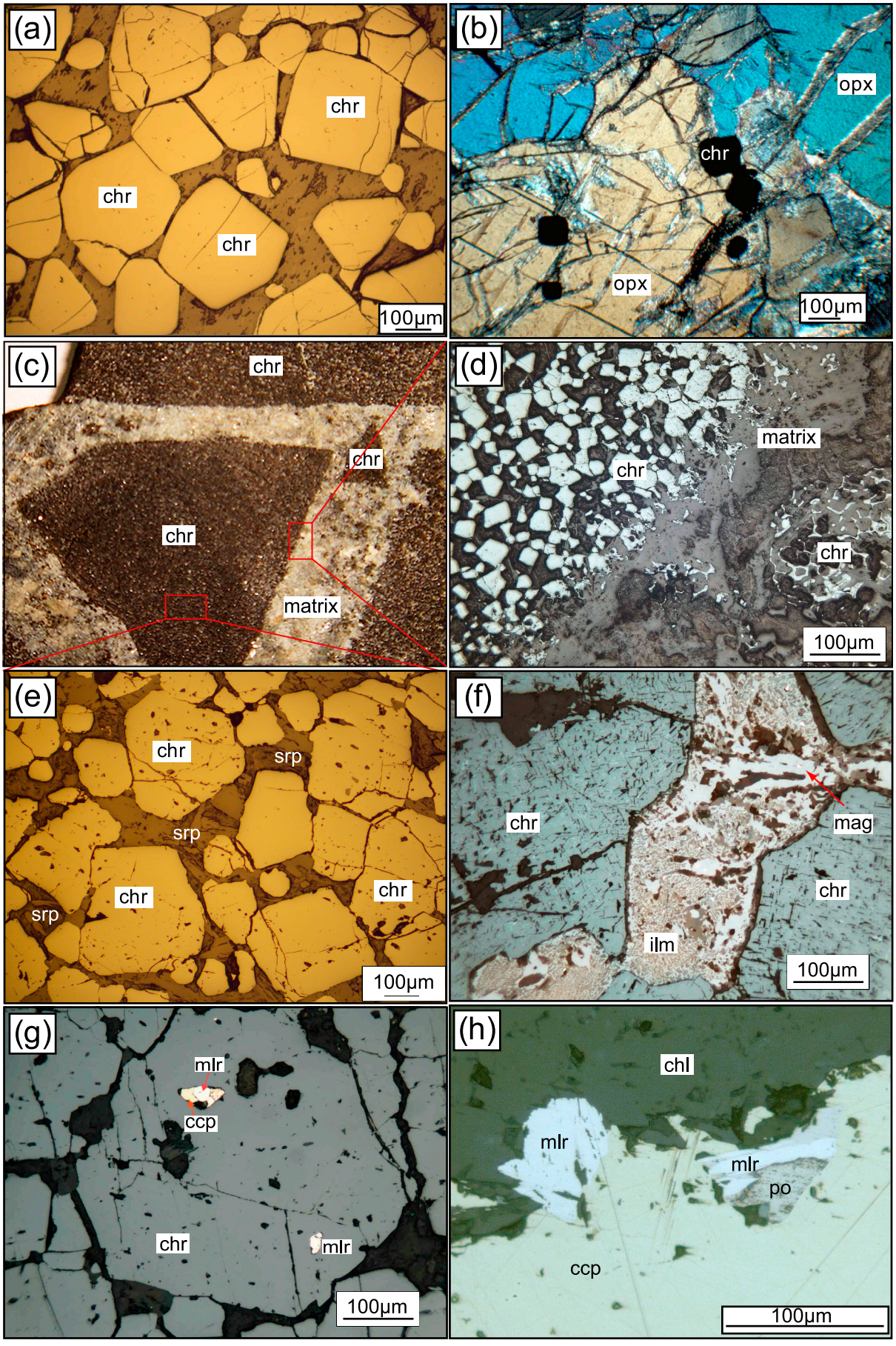

(caption on next page)

Fig. 3. Photomicrographs showing textures of different rocks in reflected light (except b, c): (a) Massive chromitite from the main ultramafic unit with subhedral to euhedral chromite (chr) grains with serpentine (after olivine) at the interstitial spaces; Sample no. SCM/39/OB2; Sample from Sukinda mine; (b) Euhedral chromite (chr) crystal poikilitically included within orthopyroxene (opx) in orthopyroxenite (transmitted light; crossed polars); Sample no. SCM/08/O2; Sample from main ultramafic unit, Sukinda mine; (c) Photograph of thin-section slide (6/4 cm) showing chromitite breccia within gabbroic matrix; (d) Part of chromitite breccia and the gabbroic matrix; Chromite (chr) grains are extensively altered within the gabbroic matrix, whereas unaltered chromites are present away from the contact between the chromitite clast and the gabbroic matrix, in the inner part of the breccia clast; Sample no. KTPL-27, Katpal area; (e) Unaltered chromite grains of chromitite clast away from the contact of gabbroic matrix; (f) Altered chromite grains within the gabbroic matrix containing needles of chlorite as inclusions; ilmenite (ilm) and magnetite (mag) intergrowths were developed along the grain contacts; (g) Coarse chromite grains of breccia clast showing corroded boundaries containing inclusions of chalcopyrite (ccp) and millerite (mlr); (h) Sulfide-rich assemblage within altered gabbroic matrix. Silicate minerals are mostly chlorite (chl) and sulfide minerals are millerite (mlr), pyrrhotite (po) and chalcopyrite (ccp).

gabbroic to granodioritic matrix forming a tectonic breccia (Figs. 2c, d, f and 3c). The breccia fragments are mostly triangular, rectangular, ellipsoidal, and sub-rounded to rounded in shape. At some places, thick dark brown rims of altered chromites are present around the chromitite fragments, and these rims are feebly magnetic. Some smaller chromitite clasts are also weakly magnetic. Chromitite clasts are dark black to brown in colour. The chromite grains in the central part of a chromitite breccia (Fig. 3c–e) are texturally similar to the chromitite ores of the main ultramafic unit (Fig. 3a). In contrast, the chromite grains in the outer part of such chromitite breccia and also in the gabbroic/granodioritic matrix materials are variably altered and have corroded boundaries (Fig. 3c–g). The altered chromite grains often contain three sets of chlorite lamellae along the crystallographic planes (Fig. 3f). An assemblage of magnetite and ilmenite is commonly developed within the altered parts of the chromitite breccia (Fig. 3f). In places chromite grains have ferritchromit ± magnetite rims along the grain boundary. The chromite grains from the chromitite breccia are characterized by grain coarsening, and sometimes contain sulfide mineral inclusions (chalcopyrite and millerite; Fig. 3g).

The gabbroic matrix of breccia consists of medium- to coarse-grained plagioclase, clinopyroxene, amphibole, serpentine, talc and quartz and can sometimes be pegmatoidal (Fig. 2d). Some chromite grains are physically incorporated within the gabbroic matrix materials of the breccia. These grains are highly fragmented and more altered than the chromites in the chromitite fragments. Sulfide minerals (chalcopyrite, millerite with minor pyrrhotite) are present sporadically as veins within the gabbroic matrix of the breccia assemblages (Fig. 3h). Minor amount of chalcopyrite is present at the interface of altered chromite grains and the silicate matrix, and sometimes altered to bornite and chalcocite.

4. Analytical methods

Representative samples of all rock suites were cleaned, crushed and pulverized to 300 mesh with a tungsten-carbide mill in the Department of Geological Sciences, Jadavpur University. Major elements analyses were performed on a Bruker S4 Pioneer wavelength dispersive (WD) XRF instrument at the National Centre for Earth Science Studies (NCESS), Trivandrum, India. Fused glass disks were used for analysis. The glass discs were prepared by fusing one gram of finely-powdered sample mixed with 5 g of lithium tetra-metaborate flux in a platinum crucible at 1100 °C using Claisse Fluxer. An in-house developed analytical programme using > 15 international standards, representative of matrix and target element concentrations, were used for calibration. The precision and accuracy of calibration curves, and data reliability are available at http://ncess.gov.in/research-groups/crustal-processes-crp-group/laboratories/xrf-lab.html. The standards DTS2B (dunite) of USGS and PMS (gabbro) were used to check accuracy. Analytical results for standard reference materials are tabulated in Annexure-B (available online). Trace elements including large ion lithophile elements (LILE), high field strength elements (HFSE) and rare earth elements (REE) were determined from solutions prepared from homogenized sample powder dissolved in reagent grade HF:HNO_3 acid mixture in Savillex® screwtop vessels. Matrix matching certified reference materials UB-N (ANRT, France), NIM-D (MINTEK, South Africa) and JP-1 (GSJ, Japan) along with couple of procedural blanks were also prepared to check accuracy and precision. Solutions were analyzed at CSIR-NGRI (National Geophysical Research Institute), Hyderabad by high-resolution inductively coupled mass spectrometer (HR-ICP-MS) (Nu Instruments Attom®, UK) in jump-wiggle mode at resolution of 300 that permits all the analytes of interest to be measured accurately. Instrument was optimized using 1 ppb tuning solution and the sensitivity of ^{114}In was about 1 million cps. Mass bias fractionation and several well-known isobaric interferences were addressed by using certified geochemical reference materials. Analytical results for standard reference materials BHVO-1 and JB-2 are tabulated in Annexure-C (available online). Bulk-rock major and trace element data for all the samples are presented in Annexure-D (available online) and the representative data are presented in Table 1. The PGE concentrations in the samples and the reference materials were determined using the NiS fire assay followed by Te co-precipitation separation and pre-concentration techniques and HR-ICP-MS (Balaram et al., 2006). Bulk-rock PGE data for representative samples are given in Table 2. Analytical results for standard reference materials are shown in Annexure-E (available online).

The platinum-group minerals (PGM) were analyzed using a Cambridge Instruments S360 scanning electron microscope (SEM) at Cardiff University. The details of the PGM analytical protocol have been discussed in Prichard et al. (2017a). Polished blocks were searched systematically for PGM using the four quadrants back scattered electron detector (4QBSD) on the SEM set at a magnification of ×100. A pure cobalt reference standard was analyzed in order to check for any drift in the analytical conditions. Images were photographed using a 4 quadrant back-scattered detector operating at 20 kV, a beam current of 500 pA and a working distance of 13 mm.

5. Results

5.1. Summary of chromite and silicate mineral chemistry

Mondal et al. (2006) have presented detailed EPMA mineral chemical data of chromites as well as common silicate minerals from both the Sukinda and Nuasahi Massifs. Olivine in the dunite (where it has not been serpentinised) and chromitite of the main ultramafic unit from the Sukinda Massif, has composition Fo_{92} (Pal and Mitra, 2004). Orthopyroxenes in the orthopyroxenite of the main ultramafic unit are magnesian-rich enstatite (% En = 89.4) with low calcium content (Mondal et al., 2006).

Accessory chromites in serpentinite (after dunite) of the main ultramafic unit from the Sukinda Massif is zoned with an outer rim of ferritchromit (e.g., Mondal et al., 2006; Mukherjee et al., 2010 and references therein), characterized by low *Mg*-ratio (*Mg*-ratio = Mg/(Mg + Fe^{2+})) (0.03–0.57) and wide variation in *Cr*-ratio (*Cr*-ratio = Cr/(Cr + Al)) (0.60–1.0) (Mondal et al., 2006). The accessory chromite in the orthopyroxenite is characterized by high *Cr*-ratio (0.75–0.82) and low *Mg*-ratio (0.11–0.17) (Mondal et al., 2006). Chromite grains in the massive chromitites have *Cr*-ratio ranging from 0.75 to 0.81, and *Mg*-ratio ranging from 0.62 to 0.73 (Mondal et al., 2006).

The composition of unaltered chromite in the massive chromitite fragments (*Cr*-ratio = 0.76–0.78 and *Mg*-ratio = 0.78–0.81; Mohanty

Table 1
Representative whole-rock major and trace element data for samples from the Sukinda Massif.

	SCM/19/OB2 serpentinite	SCM/111/OB2 serpentinite	SCM/08/02 ortho-pyroxenite	KTPL/22 peridotite	KTPL/36 pegmatitic gabbro	KTPL/56 Pegmatitic gabbro	KTPL/9 basalt
wt.%							
SiO_2	43.82	47.08	56.36	51.93	57.96	49.36	53.76
TiO_2	0.07	0.03	0.04	0.44	1.63	2.44	0.59
Al_2O_3	1.32	1.11	0.80	6.48	10.67	11.02	13.65
$Fe_2O_{3(t)}$	7.25	5.70	7.73	13.51	7.55	17.65	11.24
MnO	0.15	0.06	0.10	0.21	0.03	0.00	0.17
MgO	47.07	45.68	34.23	19.43	8.76	8.69	8.30
CaO	0.03	0.04	0.61	7.93	7.71	7.19	10.25
Na_2O	0.00	0.00		0.00	4.65	2.46	1.02
K_2O	0.01	0.00	0.00	0.03	0.03	0.92	0.59
P_2O_5	0.00	0.00	0.00	0.04	1.02	0.27	0.09
LOI	14.00	13.00	0.42	4.76	0.66	1.93	2.51
Total	99.73	99.71	99.88	100.00	100.00	100.00	99.66
ppm							
Sc	1.14	1.52	10.04	28.45	54.70	69.06	19.03
V	26.38	19.31	47.42	168.77	179.62	526.82	241.62
Cr	4039	4178	4907	2449	1651	7990	1244
Co	112.96	38.04	77.91	91.19	33.23	73.54	54.12
Ni	2131	2275	597.66	1023	128.41	238.20	214.68
Cu	0.46	2.71	20.67	73.42	45.33	342.12	63.76
Zn	9.09	7.17	56.97	104.32	62.01	145.59	143.32
Ga	0.63	1.50	1.81	14.06	12.97	23.76	26.06
Rb	0.28	0.13	0.80	1.51	0.87	28.72	28.86
Sr	0.00	0.10	4.21	14.98	122.37	274.46	153.35
Y	0.22	0.13	0.53	9.31	85.73	37.46	20.10
Zr	2.25	1.05	1.95	24.35	278.46	212.62	41.35
Nb	–	–	–	–	–	–	–
Cs	0.02	0.04	0.03	0.15	0.27	1.47	0.86
Ba	0.02	0.04	10.64	20.72	37.68	268.90	129.76
La	0.11	0.04	0.24	2.07	98.08	20.68	10.44
Ce	0.26	0.08	0.42	5.72	169.66	39.76	20.49
Pr	0.03	0.01	0.05	0.85	20.58	5.41	2.83
Nd	0.13	0.04	0.20	4.02	85.38	24.60	11.82
Sm	0.03	0.01	0.06	1.14	16.56	5.95	2.64
Eu	0.01	0.00	0.02	0.43	2.30	2.00	0.82
Gd	0.04	0.02	0.07	1.47	17.50	6.21	3.50
Tb	0.01	0.00	0.01	0.28	2.85	1.17	0.60
Dy	0.04	0.03	0.08	1.62	12.56	5.48	3.27
Ho	0.01	0.01	0.03	0.37	2.52	1.13	0.73
Er	0.03	0.02	0.07	1.01	8.20	3.81	2.24
Tm	0.00	0.00	0.01	0.17	1.06	0.53	0.34
Yb	0.03	0.02	0.08	0.94	6.45	3.26	2.02
Lu	0.00	0.00	0.02	0.15	1.00	0.51	0.32
Hf	0.08	0.03	0.05	0.58	6.77	4.67	0.86
Ta	–	–	–	–	–	–	–
Pb	0.04	0.04	8.16	11.15	8.45	5.96	6.67
Th	0.01	0.01	0.10	0.45	16.94	3.55	0.12
U	0.08	0.13	0.11	0.23	2.20	0.97	0.10

	SCM/39/OB2 massive chromitite	SCM/68/OB2 massive chromitite	KTPL/12 chromitite fragment	KTPL/21 chromitite fragment	KTPL/26 chromitite fragment	KTPL/27 breccia	KTPL/52 breccia	T/2 breccia
ppm								
Sc	7.97	11.74	2.65	8.90	9.34	19.07	27.03	52.10
V	20.60	41.37	64.24	190.95	28.15	88.98	274.69	844.08
Cr	–	–	–	–	–	–	–	–
Co	5.94	4.56	59.04	65.21	24.01	17.85	47.12	103.57
Ni	618.95	307.06	1581	714.78	1496	476.91	931.86	462.70
Cu	19.89	15.70	26.32	38.13	33.12	130.34	198.68	85.07
Zn	48.38	43.12	59.50	132.72	91.23	118.08	124.58	111.33
Ga	1.35	2.38	1.02	9.54	2.11	5.58	15.99	16.67
Rb	0.77	0.62	0.69	1.58	3.46	1.81	1.90	4.48
Sr	7.42	2.87	5.04	6.48	6.18	12.37	19.25	49.82
Y	1.94	0.52	1.14	3.50	2.34	8.89	13.20	21.44
Zr	4.99	4.92	2.56	6.07	10.16	9.77	12.38	22.39
Nb	–	–	–	–	–	–	–	–
Cs	0.03	0.05	0.03	0.05	0.13	0.12	0.13	0.12
Ba	22.92	8.89	10.08	8.77	13.36	20.06	13.34	77.07
La	0.46	0.49	1.25	0.77	1.09	2.51	3.34	4.58
Ce	1.24	0.85	2.83	2.05	2.39	7.08	10.38	13.29
Pr	0.18	0.12	0.31	0.33	0.30	1.01	1.60	1.95
Nd	0.74	0.47	0.98	1.54	1.17	4.71	7.12	8.97
Sm	0.20	0.11	0.18	0.40	0.26	1.21	1.58	2.45

(*continued on next page*)

Table 1 (*continued*)

	SCM/39/OB2 massive chromitite	SCM/68/OB2 massive chromitite	KTPL/12 chromitite fragment	KTPL/21 chromitite fragment	KTPL/26 chromitite fragment	KTPL/27 breccia	KTPL/52 breccia	T/2 breccia
Eu	0.06	0.03	0.03	0.10	0.09	0.53	0.76	0.74
Gd	0.27	0.14	0.21	0.54	0.35	1.54	2.17	3.34
Tb	0.05	0.02	0.03	0.11	0.06	0.28	0.39	0.64
Dy	0.32	0.12	0.20	0.56	0.39	1.60	2.27	3.80
Ho	0.08	0.02	0.04	0.14	0.09	0.35	0.54	0.87
Er	0.21	0.08	0.13	0.37	0.25	1.00	1.46	2.36
Tm	0.04	0.02	0.02	0.06	0.05	0.16	0.25	0.40
Yb	0.22	0.08	0.11	0.35	0.23	0.87	1.28	2.11
Lu	0.04	0.01	0.02	0.06	0.04	0.14	0.21	0.35
Hf	0.12	0.09	0.07	0.14	0.22	0.27	0.37	0.84
Ta	–	–	–	–	–	–	–	–
Pb	10.36	4.73	10.58	9.45	9.50	11.08	8.72	8.67
Th	0.10	0.01	0.09	0.11	0.32	0.21	0.29	0.48
U	0.11	0.07	0.16	0.15	0.11	0.15	0.17	0.19

nd: not determined; – not reported; Analysis of major elements from NCESS, MoES (Trivandrum, India); trace element analysis from CSIR-NGRI (Hyderabad, India); note that the analyses are reported on an anhydrous basis and LOI values for information purpose. Analysis of trace element from CSIR-NGRI (Hyderabad, India); major elements are not determined for chromitites.

Table 2
PGE concentration in ppb, in the Sukinda rocks.

	SCM/43/OB2 serpentinite	SCM/33/OB2 serpentinite	SCM/112/OB2 serpentinite	SCM/140/OB2 serpentinite	SCM/08/02 ortho-pyroxenite	SCM/08/08 ortho-pyroxenite	KTPL/22 peridotite	KTPL/28 pegmatitic gabbro	KTPL/36 Pegmatitic gabbro
ppb									
Os	12.8	3	1	5.4	0.8	0.6	0.8	0.4	2.6
Ir	12.2	2.2	1.2	3.8	0.6	0.6	0.2	0.2	0.4
Ru	23	7.2	10	20	7.2	4.4	3.6	2.4	3.2
Rh	0.6	0.4	1	1	0.2	0.6	0.4	0.2	0.4
Pt	20.4	5	3.4	4.8	9.8	5.8	1.4	5.6	2.4
Pd	1.8	2.4	2	4.2	0.8	1.8	4	3.6	2.4
PPGE	22.8	12.4	6.4	10	10.8	8.2	5.8	9.4	5.2
IPGE	48	7.8	12.2	29.2	8.6	5.6	4.6	3	6.2
Total	70.8	20.2	18.6	39.2	19.4	13.8	10.4	12.4	11.4
Pt/Pd	11.33	2.08	1.70	1.14	12.25	3.22	0.35	1.56	1.00
Pd/Ir	0.15	1.09	1.67	1.11	1.33	3	20	18	6

	KTP/170 gabbro	KTPL/9 basalt	KTPL/11 basalt	SCM/39/OB2 massive chromitite	SCM/68/OB2 massive chromitite	SCM/106/OB2 massive chromitite	SCM/114/OB2 massive chromitite	*SCM/13/80 massive chromitite	*SCM/13/83 massive chromitite
ppb									
Os	0.6	0.6	1	66.4	193	7.6	25.2	121	46
Ir	0.2	0.4	0.4	46.8	180.6	84.8	29.2	188	74
Ru	2	3	3.2	75	260	208.6	99.8	219	212
Rh	0.6	0.8	1	2.6	12.6	8.8	6	13	14
Pt	3.8	12.6	14.8	14.4	51.8	20	11.4	84	496
Pd	1.8	11.6	12.6	2.8	28.4	1.6	4.2	26	33
PPGE	6.2	25	28.4	19.8	92.8	30.4	21.6	123	332
IPGE	2.8	4	4.6	188.2	633.6	301	154.2	528	543
Total	9	29	33	208	726.4	331.4	175.8	651	875
Pt/Pd	2.11	1.09	1.17	5.14	1.82	12.50	2.71	3.23	0.14
Pd/Ir	9	29	31.5	0.06	0.16	0.02	0.14	0.14	0.45

	KTPL/12 chromitite fragment	KTPL /15 chromitite fragment	KTPL/21 chromitite fragment	KTPL/26 chromitite fragment	KTPL/19 breccia	KTPL/27 breccia	KTPL/41 breccia	KTPL/52 breccia	T/2 breccia
ppb									
Os	26.4	51.6	89	22.6	28.8	25.8	6.4	17.2	1.4
Ir	26.8	37.6	52.6	11.8	24.8	16.4	8.8	14.8	0.6
Ru	30.8	129.8	60.6	15.2	50	47.2	16	16	5.6
Rh	1.8	7	1.6	0.6	1.2	4	0.6	0.6	0.4
Pt	15.6	28.8	15.4	9	12.8	19.2	9.8	11.8	5.4
Pd	2	24.4	1.6	1.4	4.6	10.6	2.4	2.2	7.8
PPGE	19.4	60.2	18.6	11	18.6	33.8	12.8	14.6	13.6
IPGE	84	219	202.2	49.6	103.6	89.4	31.2	48	7.6
Total	103.4	279.2	220.8	60.6	122.2	123.2	44	62.6	21.2
Pt/Pd	7.80	1.18	9.63	6.43	2.78	1.81	4.08	5.36	0.69
Pd/Ir	0.07	0.65	0.03	0.12	0.19	0.65	0.27	0.15	13

PGE analyses by Ni-sulfide fire-assay followed by ICP-MS; *Analysis from GNALYSIS (Perth, Australia); rest are from CSIR-NGRI (Hyderabad, India).

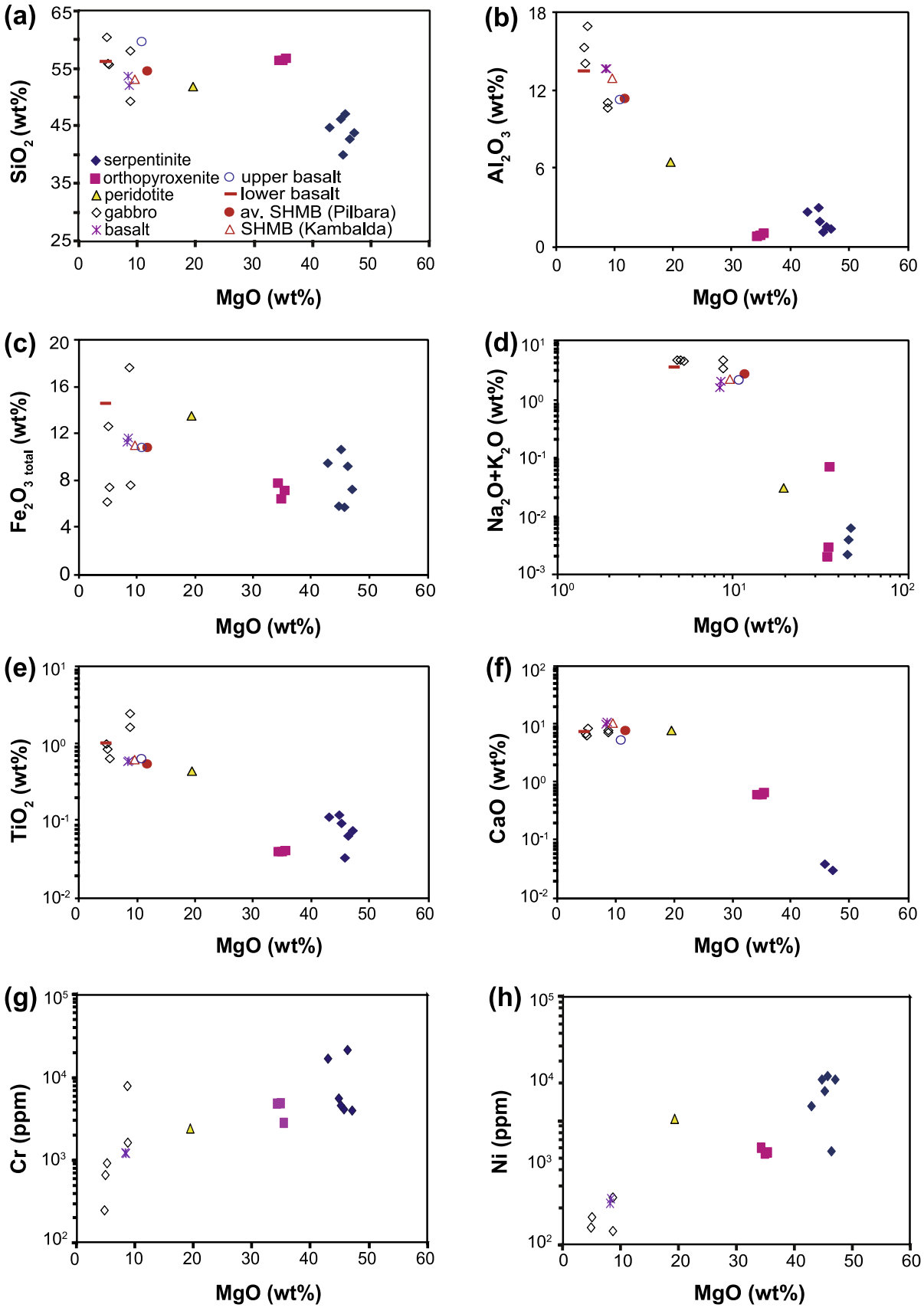

Fig. 4. Plots (a–h) of MgO content versus other major oxides and trace elements for the studied rocks from the Sukinda Massif. Average data of siliceous high-Mg basalt (SHMB) of Negri volcanic, Pilbara and SHMB of Kambalda, Western Australia from Sun et al. (1989); upper and lower basalt of the Sukinda valley from Basu et al. (1997).

and Sen, 2008) of the Katpal breccia is similar to that in the massive chromitites (*Cr*-ratio = 0.75–0.81, and *Mg*-ratio = 0.62–0.73) from the main ultramafic unit (e.g., Mondal et al., 2006). However, highly variable compositions are noted in some chromitite fragments/clasts that represent altered chromites (Raju et al., 2007). This observation is similar to that from the Nuasahi breccia zone (e.g., Mondal et al., 2001; Mondal and Zhou, 2010).

5.2. Bulk-rock geochemistry: Major and trace elements

In the bivariate plots for bulk-rock major elements there is an overall decrease of MgO with increasing SiO_2, Al_2O_3, $Fe_2O_{3(total)}$, CaO, TiO_2, and $Na_2O + K_2O$ (Fig. 4a–f). All samples show positive correlation between Ni, Cr and MgO (Fig. 4g and h). In the bivariate plots total rare-earth elements, La and Sr show positive correlation with Zr (Fig. 5a–c). All samples show negative correlation between Cu and MgO and positive correlation between Zr, Ti and Cu (Fig. 5d–f). In the Cu versus Pd, Pt and Ni versus Pd, Pt plots samples of the breccia and gabbros from Katpal area show linear relation (Fig. 6a–d).

Two samples of basalt from the Katpal area are plotted along with other samples in all the bivariate plots (Figs. 4–6). The previously reported (Basu et al., 1997) lower and upper basalts of the Sukinda Massif, and also the compositions of the Archean siliceous high-Mg basalt from the Pilbara and Kambalda greenstone belts are plotted in these bivariate plots. The compositions of basalt of this study are comparable to the previous study and the Archean siliceous high-Mg basalts. In a conventional TAS diagram (total alkali vs. SiO_2) basaltic samples of this and previous studies also show the compositional similarity with the Archean siliceous high-Mg basalt (Fig. 7).

Chondrite-normalized REE plots are shown in Fig. 8. Other than two samples serpentinites (after dunite) from the main ultramafic unit display slight LREE enrichment (≈2–3 × chondrite) with a flat to slightly upward sloping (Gd to Lu) HREE pattern (Fig. 8a). Two samples of the serpentinite are relatively REE depleted than the other samples. Most of

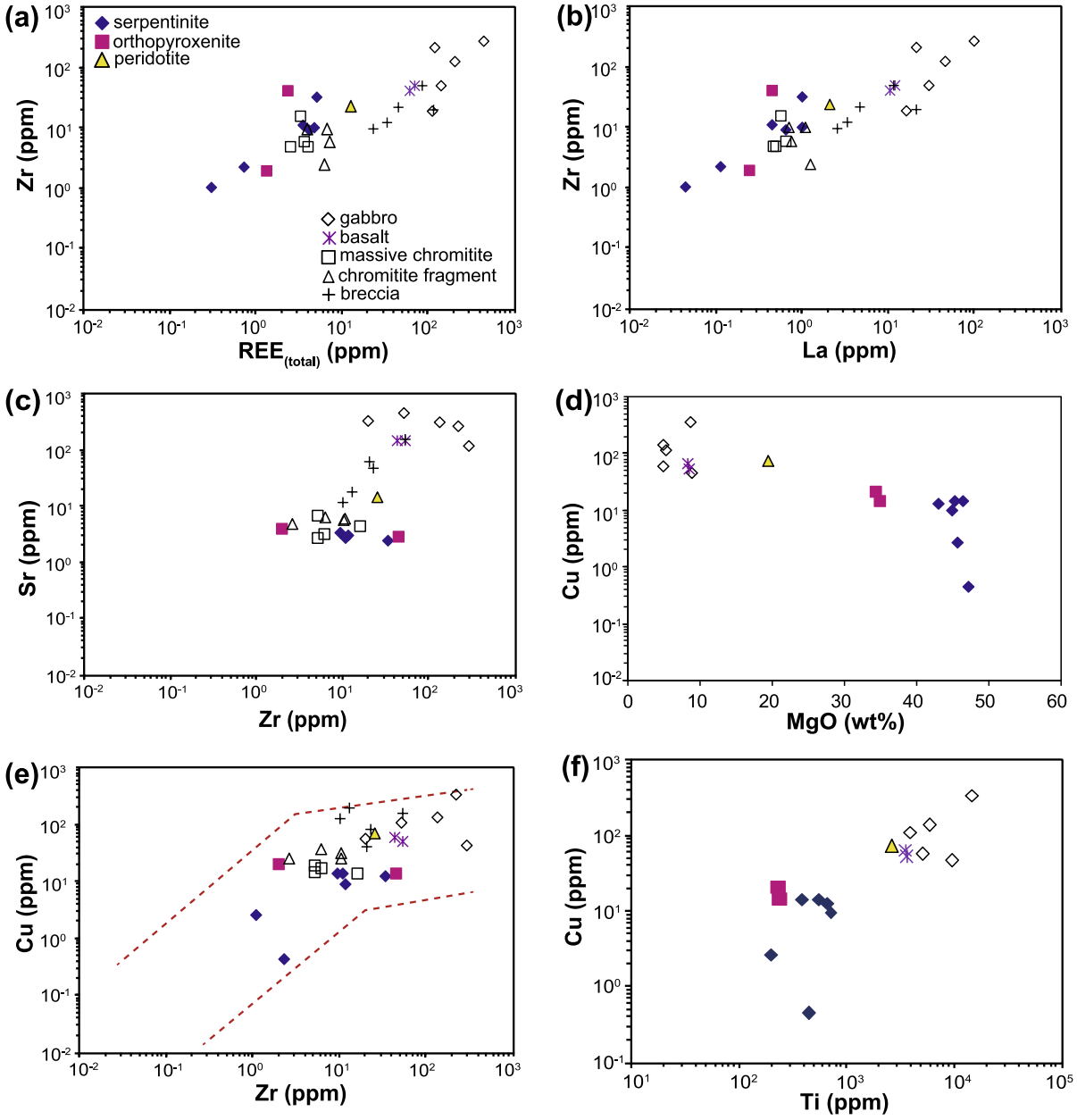

Fig. 5. Plots of (a) total REE versus Zr, (b) La versus Zr, (c) Zr versus Sr, (d) MgO versus Cu, (e) Zr versus Cu, and (e) Ti versus Cu variations in the rocks from the Sukinda Massif.

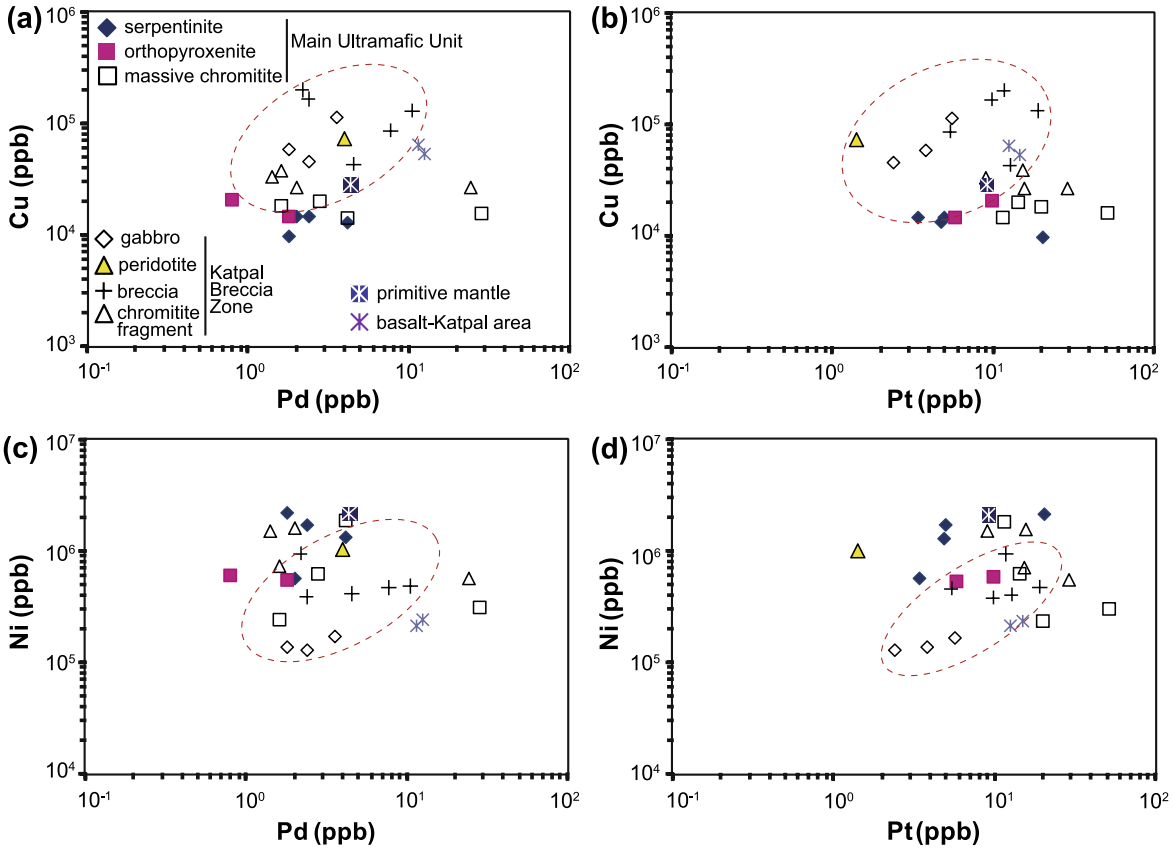

Fig. 6. Plots of (a) Pd versus Cu, (b) Pt versus Cu, (c) Pd versus Ni and (d) Pt versus Ni variations in the rocks from the Sukinda Massif.

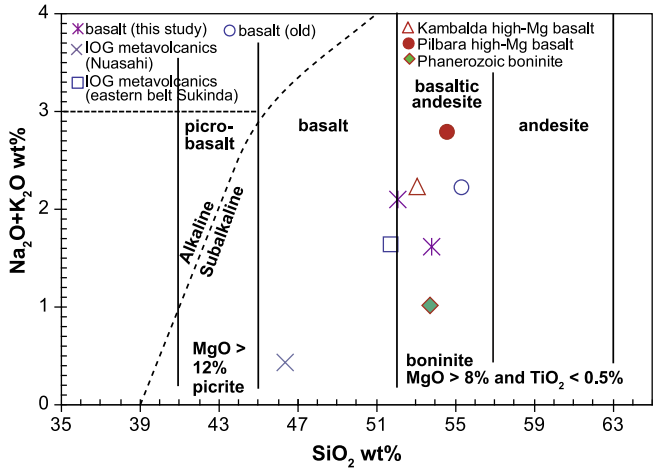

Fig. 7. Total alkali-silica diagram for high-Mg volcanic rocks (after Le Bas, 2000). Basalt (old) from Sengupta et al. (1997); IOG metavolcanics (Nuasahi) from Mondal (2000); IOG metavolcanics, eastern belt (Sukinda) from Sengupta et al. (1997); Kambalda high-Mg basalt and Pilbara high-Mg basalt from Sun et al. (1989); Phanerozoic boninite of Cape Vogel from Cameron et al. (1983).

the serpentinites have a notable negative Eu anomaly except for these two samples. The chondrite-normalized REE patterns for the orthopyroxenite from the main ultramafic unit display minor LREE enrichment (≈0.5–2 × chondrite) with slight upward (Gd to Lu) sloping HREE (Fig. 8a). Overall, the orthopyroxenites show U shape patterns with LREE enrichment with LREE/MREE > 1 mostly like the serpentinite but at concentration intermediate between the depleted serpentinite and the undepleted serpentinite (Fig. 8a). The peridotitic sample from the Katpal area has an elevated chondrite normalized REE (≈10 × chondrite) than the serpentinite and orthopyroxenite of the main ultramafic unit. The chromitites from the main ultramafic unit show slight LREE enrichment and a negative Eu anomaly like the serpentinites (Fig. 8b), whereas, samples of the chromitite fragments from the Katpal breccia zone show LREE fractionated patterns (≈2–5 × chondrite, Fig. 8c). The bulk samples of the breccia from the Katpal breccia zone, having smaller sized chromitite clasts plus the gabbroic matrix, show overall REE enrichment relative to the chromitite, serpentinite and orthopyroxenite of the main ultramafic unit (Fig. 8c). Other than two samples (≈50–100 × chondrite) the bulk samples of breccias, in general, have slight LREE enrichment (≈9–20 × chondrite) with a similar HREE pattern like the large chromitite fragments. The gabbro and the basalt from the Katpal area are overall REE enriched (Fig. 5a; Table 1; Annexure-D) and the patterns are very similar but at higher concentration with overall elevated REE (LREE ≈ 45–400 × chondrite and HREE ≈ 30–90 × chondrite; Fig. 8d).

In the chondrite-normalized spidergrams the breccias and the large chromitite fragments of the Katpal breccia zone show enrichment of all elements relative to the rocks of the main ultramafic unit (Fig. 8e–h). Overall, the gabbro and the basalt from the Katpal area as well as samples of the breccia are Zr and Hf enriched (≈3–70 × chondrite) than the samples of the lower ultramafic unit including the massive chromitites (≈0.3–10 × chondrite). In the spidergrams the Zr and Hf are showing positive anomalies in serpentinite, orthopyroxenite and in one sample of the chromitite from the main ultramafic unit (Fig. 8e and f). Other two samples of the chromitite from the main ultramafic unit are characterized by slight positive Zr anomalies but without the Hf anomalies (Fig. 8f). Other than one sample of chromitite fragment and one gabbro all samples from the Katpal breccia zone representing chromitite fragment, breccia, and gabbro are showing negative Zr and Hf anomalies (Fig. 8g and h). Two samples of basalt from the Katpal area are also characterized by negative Zr and Hf anomalies (Fig. 8h).

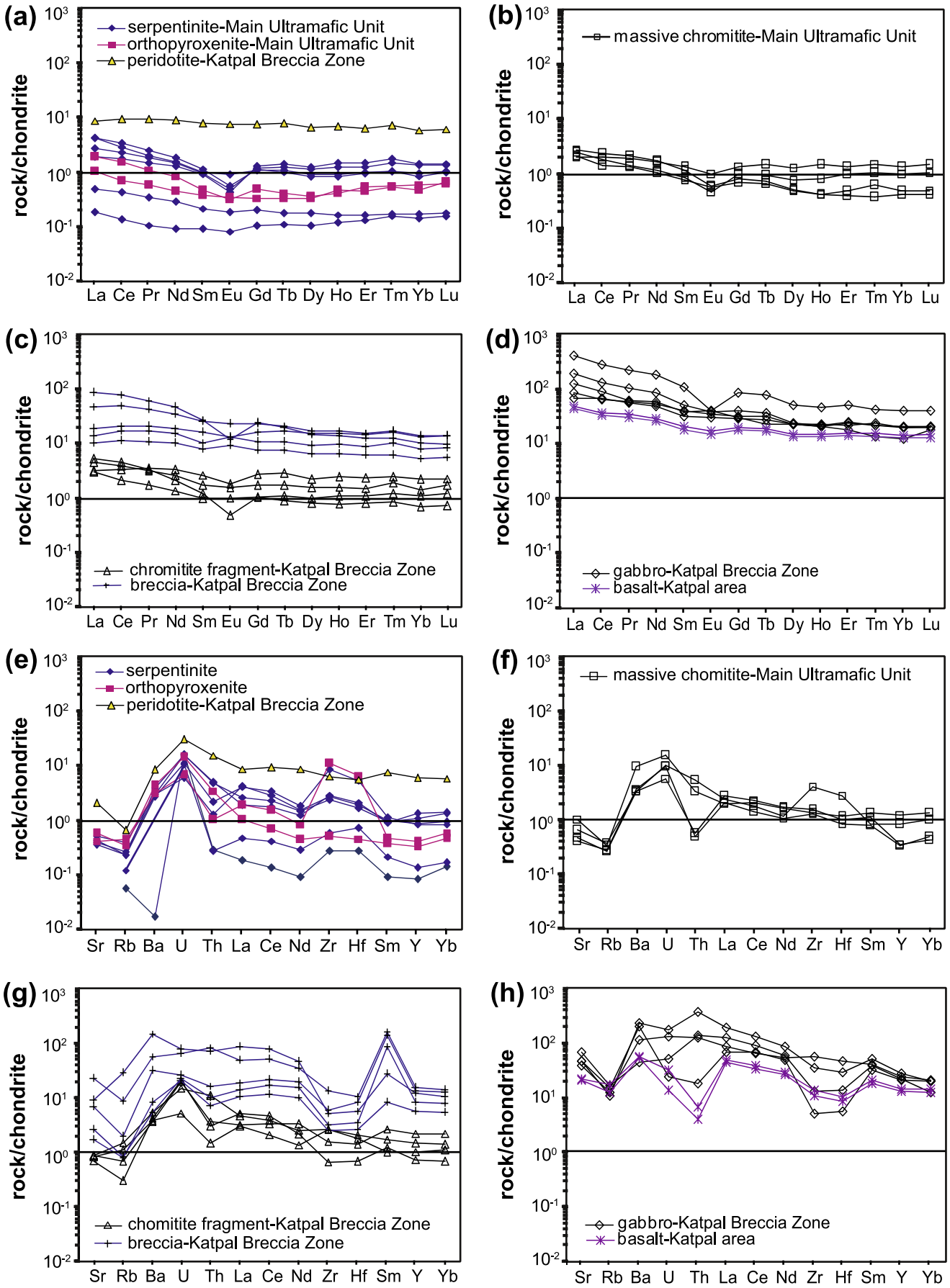

Fig. 8. (a)–(d) Chondrite-normalized REE and (e)–(h) trace element patterns for ultramafic (including chromitites), mafic and breccia rocks form the Sukinda Massif. Chondrite data from McDonough and Sun (1995).

These two samples are also showing strong negative Th anomaly like few samples of the Katpal breccia zone representing chromitite fragment, breccia and gabbro. Two samples of the chromitite and few from the serpentinite and orthopyroxenite are also showing negative Th anomalies (Fig. 8a and b).

5.3. Bulk-rock platinum-group elements geochemistry (PGE)

In the bivariate plots, IPGE (Ir, Os, Ru) show positive correlations with MgO but PPGE (Pd, Pt, Rh) show a flat distribution i.e. not much PPGE variation with MgO (Fig. 9). The IPGE show strong positive relation with Cr, whereas Rh shows a weak positive relation with the Cr (Fig. 10a–d). In contrast, Pt and Pd do not exhibit any convincing correlation with Cr in most of the rocks other than for the breccias from Katpal; the samples of the breccia show negative correlation in the Pd versus Cr plot (Fig. 10f).

The massive chromitites from the main ultramafic unit and the chromitite fragments from the Katpal area have elevated PGE concentrations than all other rocks in the Sukinda Massif (Fig. 11, Table 2). The samples of the massive chromitites from the main ultramafic unit have higher PGE concentrations than the massive chromitite fragments of the Katpal breccia (e.g., 175.8–726.4 ppb vs. 60.6–279.2 ppb). Two samples (SCM/13/80 and SCM/13/83) of the lowermost chromitite band (**CB 1**) and one sample (SCM/68/OB2) from the second band (**CB 2**) of the main ultramafic unit have higher PGE than the other samples analyzed from the Sukinda Massif (Table 2). The samples of the breccia (chromitite clast plus gabbroic matrix) from Katpal have relatively higher concentrations of total PGEs than the samples of the serpentinite and orthopyroxenite from the main ultramafic unit (e.g., 21.2–123.2 ppb vs. 13.8–70.8 ppb; Fig. 11, Table 2).

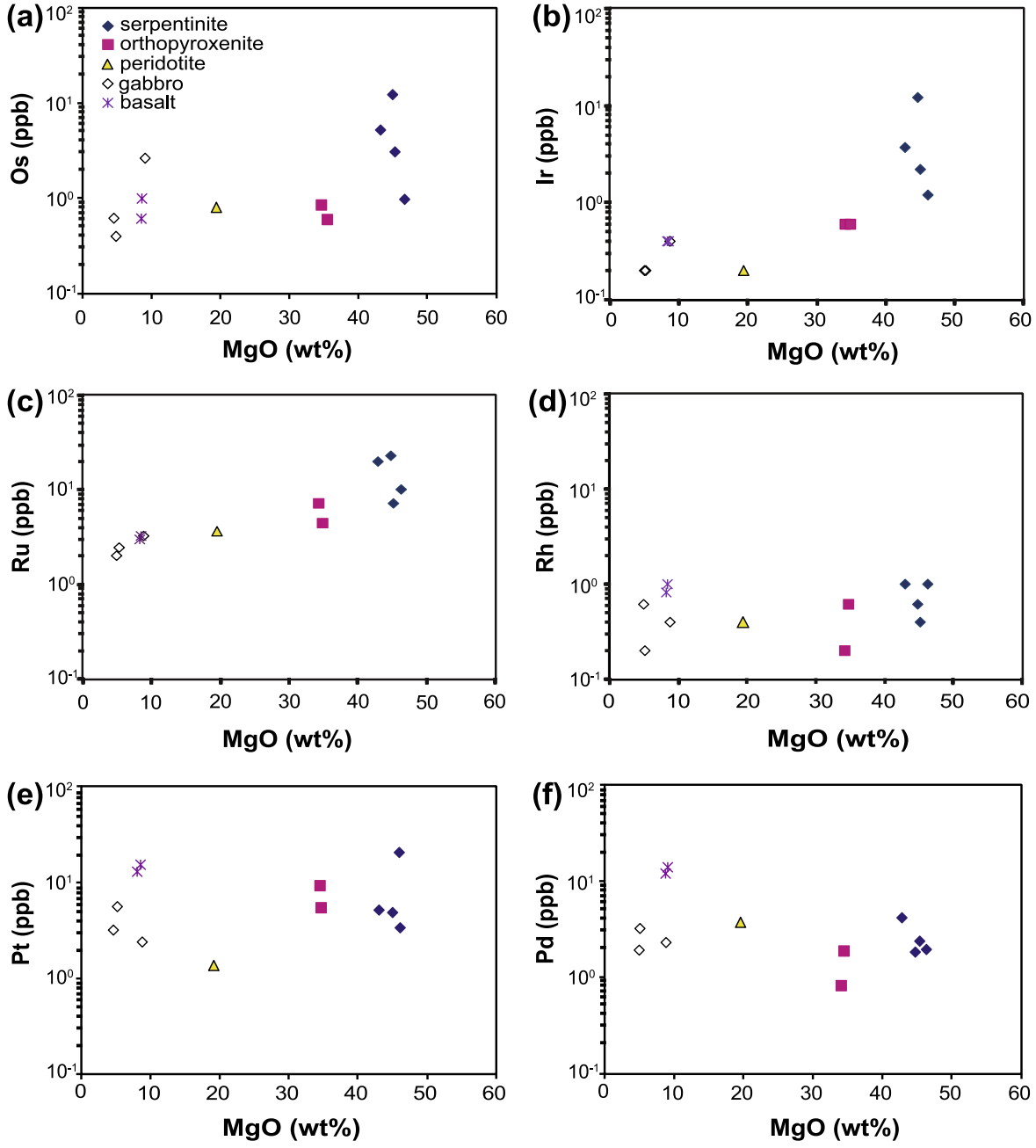

Fig. 9. Plots (a–f) of MgO content versus platinum-group element (PGE) for the rocks of the Sukinda Massif. Os, Ir and Ru show positive relations with MgO content of the rocks (a–c).

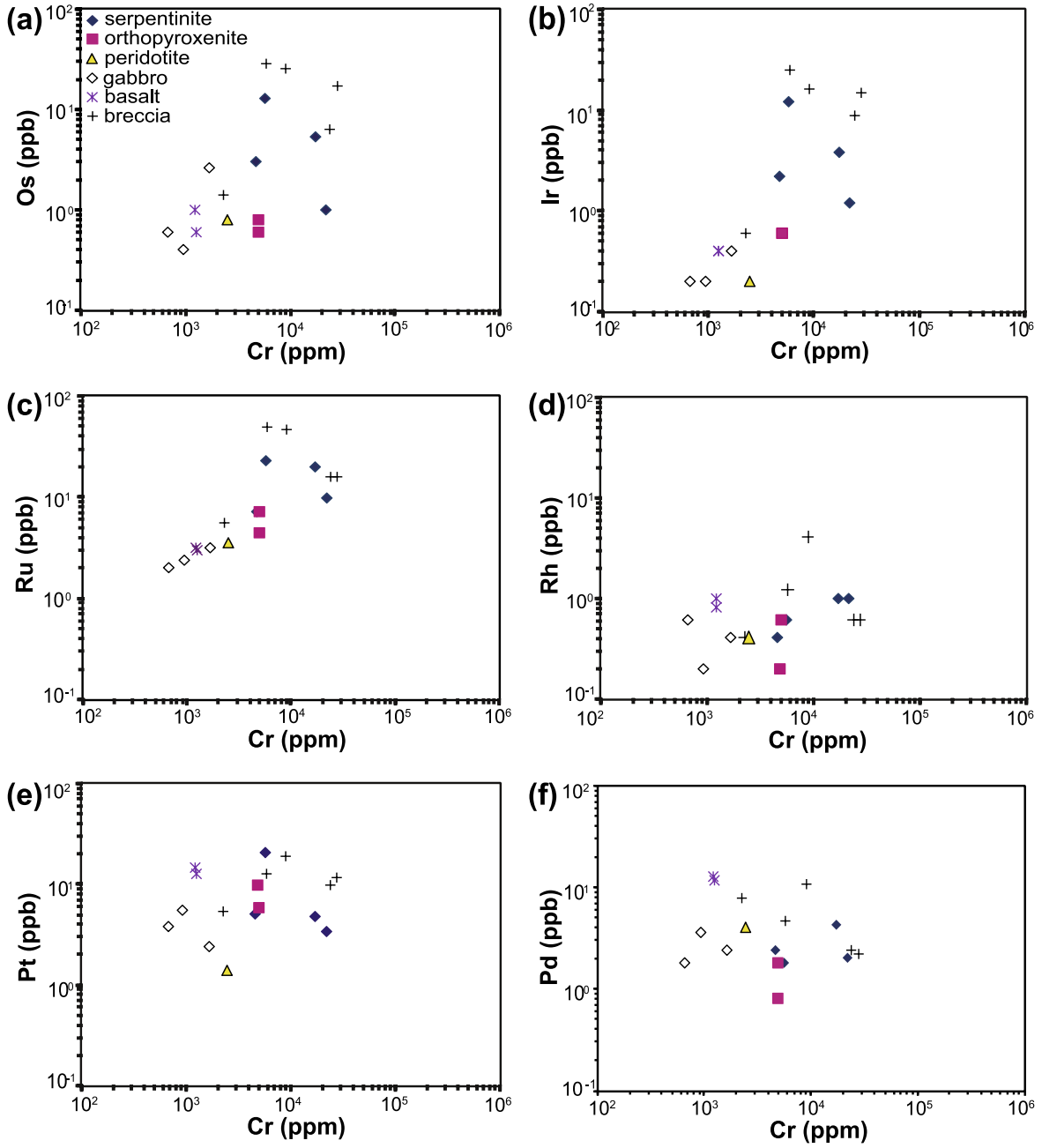

Fig. 10. Plots (a–f) of Cr content versus platinum-group element (PGE) for the rocks of the Sukinda Massif. Os, Ir and Ru show positive relations with Cr content of the rocks (a–c).

Other than one sample of serpentinite (Pt/Pd ≈ 11.33), one from orthopyroxenite (Pt/Pd ≈ 12.25) and two from the chromitites (Pt/Pd ≈ 5.14 and 12.50) all samples from the main ultramafic unit representing serpentinite, orthopyroxenite and chromitites have Pt/Pd ratios similar to or lower than the primitive mantle (e.g. serpentinite Pt/Pd ≈ 1.14–2.08, orthopyroxenite Pt/Pd ≈ 3.22 and chromitites Pt/Pd ≈ 1.82–2.71; primitive mantle = 2.09; Barnes et al., 1988b) (Fig. 11a, Table 2). Samples from Katpal area representing peridotite, breccias (clast plus gabbroic matrix) and chromitite fragments have highly variable Pt/Pd ratios (e.g., Pt/Pd ≈ 0.35–9.63). Three samples of the gabbro from Katpal have Pt/Pd ratios (Pt/Pd ≈ 1.00–2.11) similar to or lower than the primitive mantle (Fig. 11a, Table 2). Two samples of the basalt from Katpal have lower Pt/Pd ratios (Pt/Pd ≈ 1.09–1.17) than the primitive mantle (Fig. 11a, Table 2).

The samples of the massive chromitite from the main ultramafic unit and the chromitite fragments from the Katpal breccia have least fractionated PGEs (e.g., massive chromitites Pd/Ir ≈ 0.02–0.45; chromitite fragments Pd/Ir ≈ 0.03–0.65) (Fig. 11b, Table 2). Other than one sample (Pd/Ir ≈ 13) of the breccia all samples have Pd/Ir ratios (Pd/Ir ≈ 0.15–0.65) similar to the massive chromitites from the main ultramafic unit and the chromitite fragments of Katpal. The serpentinite and orthopyroxenite from the main ultramafic unit have variable Pd/Ir ratios (Pd/Ir ≈ 0.15–3.00). The samples of the peridotite and gabbro from Katpal have strong fractionated PGEs (Pd/Ir ≈ 6–20). The samples of the basaltic rocks also have strong fractionated PGEs (Pd/Ir ≈ 29–31.5) like the gabbros (Fig. 11b, Table 2).

In the primitive mantle-normalized PGE plots (Fig. 12a), two samples of the serpentinite from the main ultramafic unit show IPGE enrichment patterns whereas other two samples show depleted PGE pattern. All these samples are characterized by positive Ru anomalies (Ru/

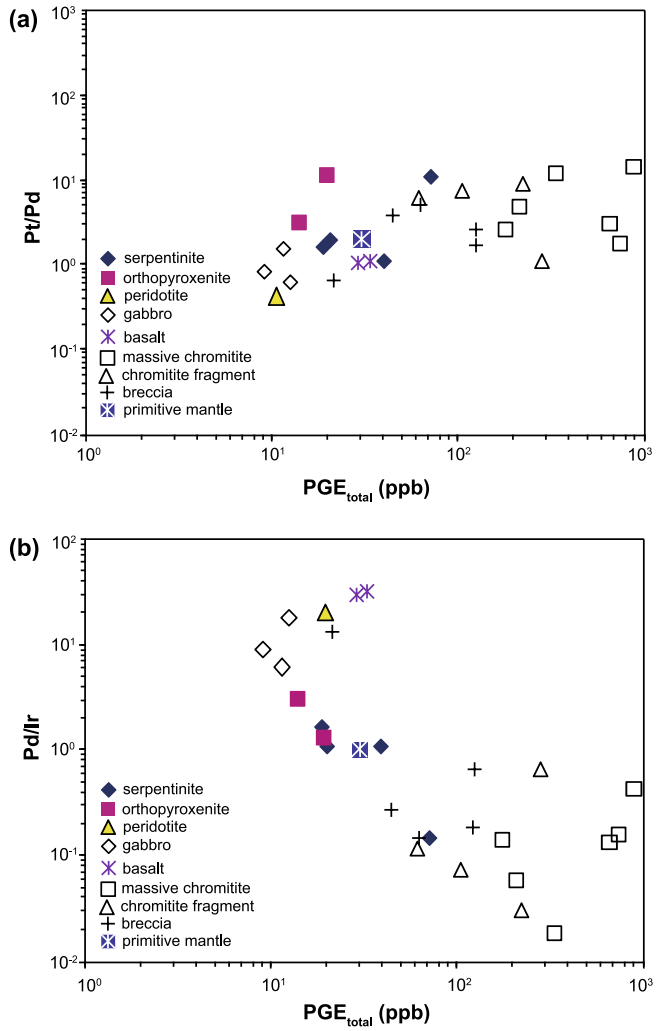

Fig. 11. Plots of (a) total PGE (ppb) versus Pt/Pd and (b) total PGE (ppb) versus Pd/Ir for the ultramafic, mafic and breccia rocks of the Sukinda Massif. Primitive mantle values from Barnes et al. (1988b).

Ir_N ≈ 1.38–6.11). One sample of the serpentinite shows a strong positive Pt anomaly (Pt/Pd_N ≈ 5.42) like the orthopyroxenite (Pt/Pd_N ≈ 1.54–5.86). The orthopyroxenites show depleted PGE patterns with positive Ru (Ru/Ir_N ≈ 5.38–8.80) anomalies (Fig. 12a). The peridotite from the Katpal area has a depleted PGE pattern with a positive Ru and a negative Ir (Ru/Ir_N ≈ 13.20) anomaly and a positive Pd anomaly (Pd/Pt_N ≈ 5.97) (Fig. 12a). The massive chromitites from the main ultramafic unit have PGE fractionated patterns with strong IPGE enrichments (≈1–50 × primitive mantle; Fig. 12b). One sample of these chromitites shows a characteristic positive Pt anomaly. The bulk sample of the breccia (chromitite clasts plus gabbroic matrix) from Katpal shows IPGE enriched patterns with positive Ru anomalies in some samples like the massive chromitite fragments (Fig. 12c). One sample of the breccia shows a depleted PGE pattern with positive Ru and Pd anomaly. The gabbro and basalt show a PPGE (Pd, Pt, Rh) fractionated pattern with negative Ir anomaly (Fig. 12d).

5.4. Platinum-group minerals (PGM)

Based on relatively higher total concentration of the PGE three massive chromitite samples (Table 2, ANNEXURE-A) of the main ultramafic unit from the Sukinda Massif were searched for PGM. Seventeen PGM were located, often composite, with 8 PGM in sample SCM/68/OB2 (PGE_{total} ≈ 726 ppb, IPGE ≈ 633 ppb, PPGE ≈ 93 ppb), 3 in sample SCM/13/80 (PGE_{total} ≈ 651 ppb, IPGE ≈ 528 ppb, PPGE ≈ 123 ppb) and 6 in sample SCM/13/83 (PGE_{total} ≈ 875 ppb, IPGE ≈ 543 ppb, PPGE ≈ 332 ppb). Most PGM occur within chromite grains (Fig. 13A–K); either totally enclosed or along altered cracks in the grains and one PGM occurs in the silicate matrix interstitial to the chromite grains (Fig. 13L). The composite PGM are small and of a very uniform size, averaging 2.5 × 2 μm in diameter with the largest 5 × 3 μm and the smallest 1 × 1 μm. They are too small for quantitative analysis but qualitative analyses were possible (Table 3). Most of the PGM are euhedral in shape (Fig. 13A–H), although they can be irregular in outline where they occur along a crack suggesting modification of their shape on alteration (Fig. 13I and J). They are all associated with silicates. Silicate inclusions containing PGM entirely enclosed by chromite, that are not near cracks, tend to be euhedral, often hexagonal and composed of single IPGE alloys rather than composite grains. The PGE assemblage is sulfur-poor with 13 Os-Ir-Ru alloys having varying element ratios from Os-rich to Ir-rich to Ru-rich (Table 3). Most of the euhedral Os-Ir-Ru alloys enclosed in chromite contain minor Pt. Two laurites were located, one in a composite grain within chromite and the other as a composite grain along a crack. Five irarsite grains occur, all associated with cracks in chromite grains. One composite grain contains a very small 2 × 0.5 μm grain of sperrylite attached to an Os-Ir-Ru alloy. All the As-bearing PGM are associated with cracks in the chromite, suggesting introduction of As during alteration that altered primary PGM to PGM-arsenides.

6. Discussion

6.1. Parental magma, and significance of major and trace element geochemistry

The ultramafic-mafic plutonic bodies like the Sukinda and Nuasahi Massifs within the Archean greenstone sequences were considered to represent sill-like layered intrusions (e.g., Mondal et al., 2001, 2006), however, their genetic relationship with the associated volcanic sequences remains uncertain (e.g., Mukherjee et al., 2012 for review). Lesher and Groves (1986) considered that plutonic ultramafic-mafic bodies within the Archean greenstone belts were originally sub-volcanic sill-like feeders to the overlying volcanic rocks that were tectonically emplaced alongside the volcanic sequences during later deformation events. An alternative hypothesis is that these ultramafic-mafic bodies represent the lower cumulates of thick komatiitic extrusions (e.g., Barnes et al., 1988a). Both Sukinda and Nuasahi Massifs in the Singhbhum craton are thin, layered sill-like igneous complexes which are characterized by thick chromitite layers. Similar thick chromitites are commonly found in the upper mantle section of the ophiolite complexes but those are essentially discontinuous, pod-shaped bodies (e.g., Arai and Miura, 2016), whereas the stratiform chromitites in a typical mafic-layered intrusion are commonly ≈ 1 m thick or less but extensive laterally (e.g., Mondal and Mathez, 2007). There is another group of chromite deposits where chromitite layers are also considerably thick (≈2–10 m thick) that includes the Inyala and Railway Block of Zimbabwe, the Ipueria-Medrado and Campo Formosa Complexes in Bahia, and the Bacuri Complex in Amapa, Brazil (e.g., Prichard et al., 2017a). In the Kemi Complex in Finland and the Black Thor in Ontario the chromitite layers are up to 100 m thick. These are chromite-rich Archean complexes and have been called 'conduit-type' (Prichard et al., 2017a and references therein). These ultramafic intrusions are in general relatively thin stratigraphically and considered to be served as conduits for high-Mg ultramafic-mafic magmas at shallow crustal levels (e.g., Mukherjee et al., 2012; Mungall, 2014). Some of these complexes are PGE-bearing as for example in the chromitites in Campo Formosa and Bacuri and in a breccia zone and in the magnetitite bands of the Nuasahi Massif (e.g., Mondal and Baidya, 1997; Prichard et al., 2017a). The Sukinda and Nuasahi Massifs in the Singhbhum craton and similar Archean chromite deposits in India such

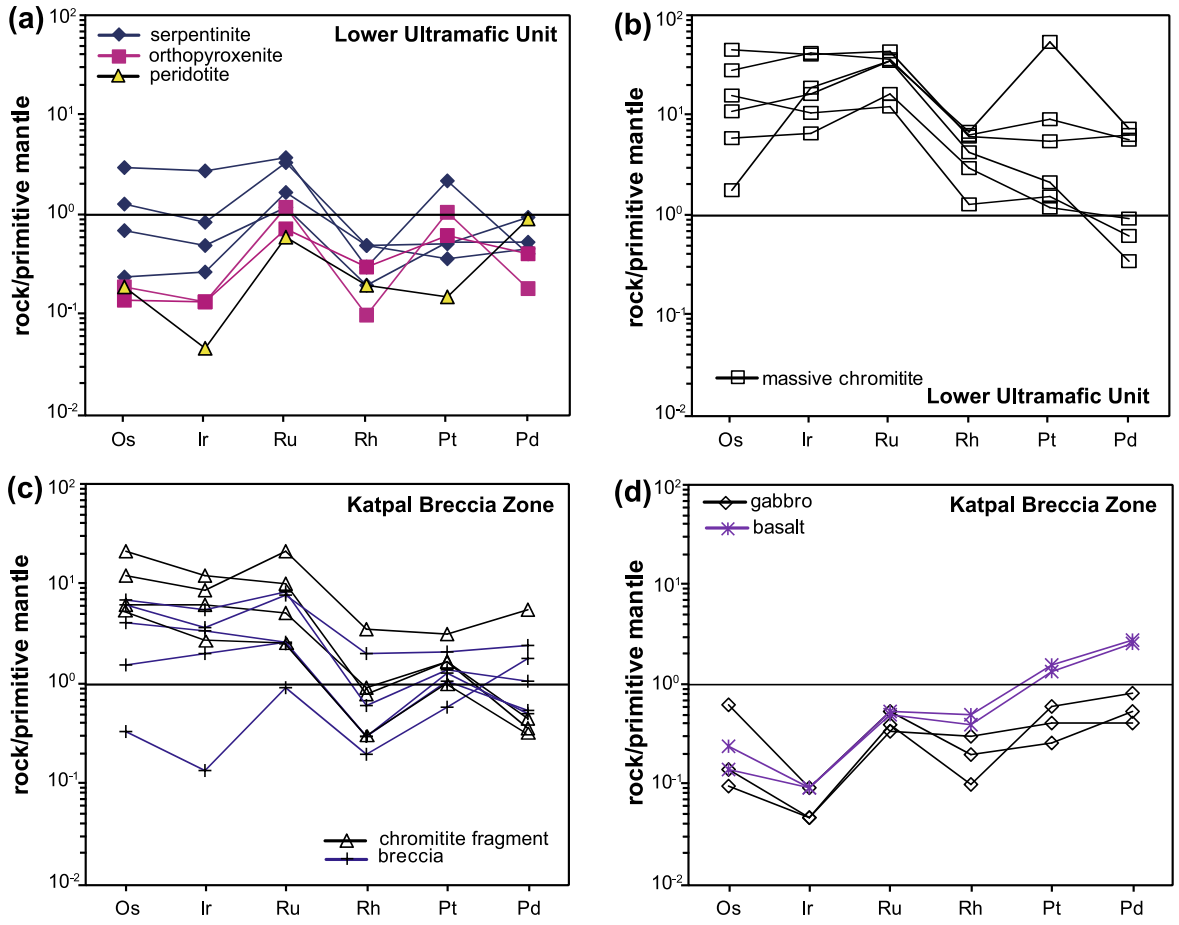

Fig. 12. Primitive mantle-normalized PGE patterns (a–d) for the samples of the Sukinda Massif. Primitive mantle values from Barnes et al. (1988b).

as the Nuggihalli Complex (Western Dharwar craton) are also 'conduit' type sill-like layered ultramafic-mafic plutonic complexes.

Based on liquidus chromite compositional plots and parental magma calculations from the massive chromitites Mondal et al. (2006) established that the ultramafic rocks including the chromitites of the Sukinda and Nuasahi Massifs were crystallized from boninitic or siliceous high-Mg basalts (SHMB) within a supra-subduction setting (Table 4). The composition of the calculated parental magma (Sukinda Massif: $Al_2O_3 \approx 10.2–11.5$ wt%, FeO/MgO ≈ 0.68–0.84; Nuasahi Massif: $Al_2O_3 \approx 10.3–11.0$ wt%, FeO/MgO ≈ 0.29–0.71) was similar to the siliceous high-Mg basaltic rocks of the Iron Ore Group supracrustals representing the Archean greenstone belts in the Singhbhum craton (Mondal et al., 2006). The parental high-Mg magma was emplaced within the crustal-volcano sedimentary sequence of the Iron Ore Group (Tomka-Daitari greenstone belt, Fig. 1b; Mondal et al., 2006). The current study shows that the major element compositions of the basaltic samples from the Katpal area are similar to the Archean siliceous high-Mg basalts (Fig. 7; Table 1, Table 4; Annexure-B). Chondrite normalized REE patterns of these basalts also have similarity with the Archean siliceous high-Mg basalts (Fig. 14a). The Archean siliceous high Mg-basalts originated by assimilation and fractional crystallization (AFC) processes involving assimilation of crustal material by komatiite magmas (e.g., Sun et al., 1989). However, the samples of the Katpal basalt are characterized by negative Zr, Hf and Th anomalies (Fig. 8h) indicating a depleted mantle source (e.g., Hofmann, 1988) and the magma was not contaminated with crustal materials. In the chondrite normalized REE plots (Fig. 8a–c) most serpentinites and massive chromitites from the main ultramafic unit along with chromitite fragments of the Katpal breccia zone have a notable negative Eu anomaly, whereas most samples of breccia, gabbro and basalt from the Katpal area are not showing any such negative Eu anomaly (Fig. 8c and d). This is also indicating a depleted mantle source for the parental magma of the ultramafic-mafic rocks of the Sukinda Massif; the mantle source became Eu depleted due to plagioclase removal in a prior melting event.

Significantly the orthopyroxenite, serpentinite and the massive chromitite from the main ultramafic unit of the Sukinda Massif shows shallow 'U' shaped chondrite normalized REE pattern with enrichment of LREE and HREE over the MREE (Figs. 8b and 14a, b). The 'U' shaped REE pattern of the ultramafic rocks is more or less similar to the Phanerozoic boninite from supra-subduction zone settings except that the boninite has much greater total REE concentrations (e.g., Hicky and Frey, 1982; Cameron et al., 1983; Crawford et al., 1989). The ultramafic rocks of the Nuasahi Massif also show similar 'U' shaped REE pattern (Fig. 14b; Khatun et al., 2014).

It has been well documented that the siliceous high-Mg basalt shows similarity in major element composition with boninite in a number of greenstone belts (e.g., Crawford et al., 1989; Barnes, 1989). Mondal et al. (2006) and Khatun et al. (2014) have summarized on this aspect and the readers are requested to refer these works for review and a brief summary is presented here. The composition of the parental magma for most of the chromite bearing ultramafic-mafic layered intrusions e.g. the Bushveld Complex (South Africa) or the Stillwater Complex (USA) are considered to be similar to lavas of boninite or high-Mg siliceous basalts (e.g., Cawthorn et al., 1981; Longhi et al., 1983; Sharpe and Hulbert, 1985). Crawford et al. (1989) proposed that boninites originate by hydrous melting of previously depleted and metasomatized mantle in supra-subduction settings. Parman et al. (2001, 2004)) argued that the siliceous high-Mg basalts are the Archean analog of modern-day boninites, and there is a close spatial association of

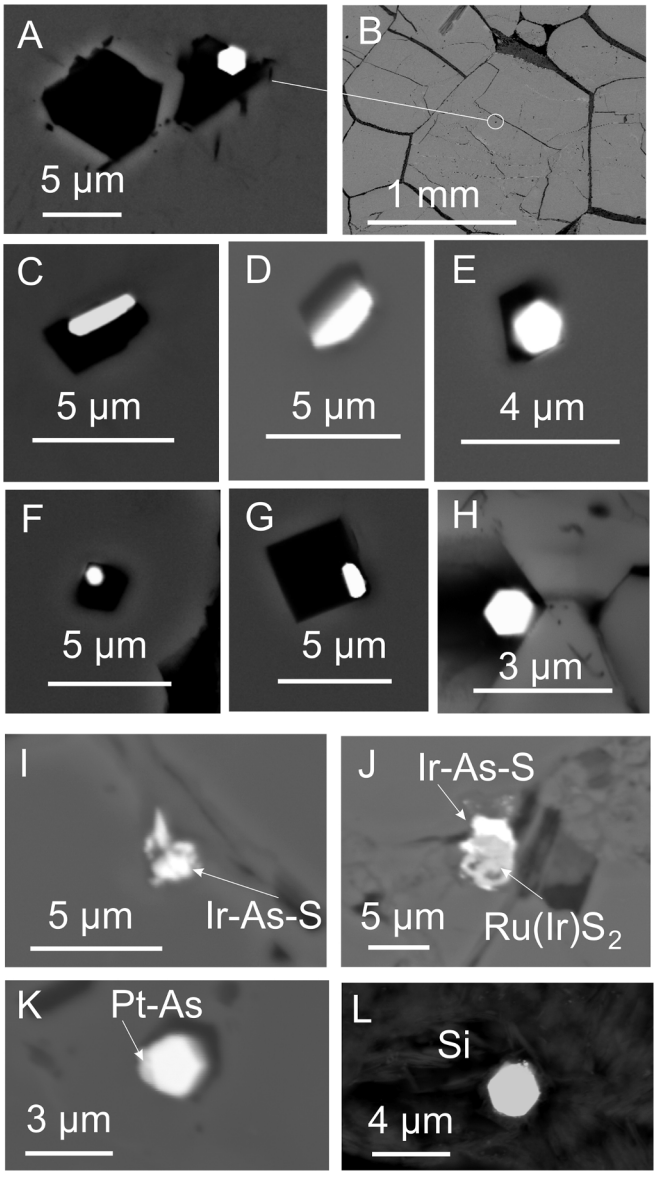

Fig. 13. Back scattered images of platinum-group mineral (PGM): (A) Ir-Os-Ru-Pt alloy in a silicate inclusion enclosed in a chromite grain, (B) Location of (A), (C)–(H) IPGE + Pt alloys in silicate inclusions in chromite, (I) Composite grain of Ir-As-S (probably irarsite) attached to an IPGE alloy adjacent to a crack in a chromite grain, (J) Composite grain of Ir-As-S (probably irarsite) attached to a laurite in a zone of alteration and cracking in chromite, (K) Composite grain of an IPGE alloy and an adjacent smaller grain of Pt-As (probably sperrylite) all in a silicate inclusion in a chromite grain, (L) Os-Ir-Ru alloy in silicate interstitial to chromite grains.

komatiite and boninite within many Archean greenstone belts (e.g., Kerrich et al., 1998). Based on petrological and experimental studies, some workers (e.g., Allègre, 1982; Grove et al., 1999; Wilson et al., 2003) suggested that some komatiites and komatiitic basalts within greenstone belts resulted from hydrous mantle melting at relatively low temperatures in supra-subduction settings in the Archean.

Previous oxygen and osmium isotopic studies by Mondal et al. (2003, 2007) on unaltered chromites from the Sukinda and Nuasahi Massifs also support that the parental magmas for these ultramafic cumulates and chromitites were not crustally contaminated. Osmium isotopic studies showed that the primary chromites from the massive chromitites in the Sukinda Massif have very unradiogenic $^{187}Os/^{188}Os$ ratios (0.10377 to 0.10536) and initial γOs values of -1.74 to -2.67 at 3.2 Ga. These features suggest derivation of the parental melts from a subchondritic source mantle domain, and the values are consistent with extraction from the subcontinental lithospheric mantle (SCLM) within the Singhbhum craton (Mondal et al., 2007).

The negative correlations between MgO versus SiO_2, Al_2O_3, CaO, TiO_2, ($Na_2O + K_2O$) and P_2O_5 suggest fractional crystallization of the parental boninitic or high Mg-siliceous basaltic magma (Fig. 4) that produced the main ultramafic unit comprising of dunite (now serpentinite), chromitite and orthopyroxenite. The linear relation (Figs. 4g, h, and 5) between the incompatible elements for samples of the main ultramafic unit and gabbro, and the chromitite breccia indicate cogenetic relationship between the rocks of the Sukinda Massif. The overall enrichment of trace elements in the breccia samples (chromitite and ultramafic clast bearing) than the samples of the main ultramafic unit (Fig. 8c and g) is due to interaction of chromitite fragments and ultramafic clasts with the evolved fractionated magma within the breccia zone from which the gabbroic matrix was formed. The rocks of the Sukinda Massif were again modified due to low-temperature hydrothermal alteration of the ultramafic-mafic rocks along with other greenstone sequences of the Iron Ore Group. Earlier O and H isotope studies of serpentine and O isotope study of the altered chromites indicate interaction with evolved seawater that resulted in this low-temperature hydrothermal alteration of the Mesoarchean ultramafic-mafic rocks (Mondal et al., 2003; Sarkar et al., 2003).

6.2. PGE fractionation from S-undersaturated boninitic magma

Other than few samples of the breccia and gabbro from Katpal area the studied rocks of the Sukinda Massif do not show evidence of base-metal-sulfide mineralization. It might be possible that the parental boninitic magma for the main ultramafic unit was not S-saturated initially, but the magma became saturated late, after considerable fractionation, when gabbroic matrix of the breccia was crystallized from the evolved magma. Sulfide is considered to be the main phase that controls the fractionation of chalcophile elements including Ni, Cu and PGEs in ultramafic-mafic magmas (Peach et al., 1990; Fleet et al., 1996; Bockrath et al., 2004). Sulfide separation from silicate magma would deplete PGEs more than the base metals, because the PGEs have much higher partition coefficients (D value) between sulfide and silicate melt than the base metals (Peach and Mathez, 1996; Fleet et al., 1999; Sattari et al., 2002; Mungall and Brenan, 2014). Rocks of the main ultramafic unit from the Sukinda Massif are not depleted in PGEs compared with Ni and Cu (Fig. 15); this indicates that the parental boninitic magma of the ultramafic unit was not S-saturated and did not experience prior sulfide removal.

A similar conclusion can be drawn from the Zr versus Cu plot (Fig. 5e); because both Cu and Zr are incompatible in normal rock forming minerals, they accumulate in residual melts during fractional crystallization of a S-undersaturated magma (Keays and Lightfoot, 2010). Cu is chalcophile and Zr is not, so, when the magma becomes S-saturated and segregates immiscible sulfides, the concentration of Cu decreases in the magma, whereas the concentration of Zr increases due to magmatic fractionation. The Zr versus Cu plots for the ultramafic rocks show more or less uniform positive trends suggesting that the parental boninitic magma was S-undersaturated and did not experience prior immiscible sulfide segregation. However, samples of the breccia and gabbros show a flat trend due to increase of Zr only, indicating fractionation of Cu with a sulfide liquid depleting the melt that was interacting with the breccias and formed the gabbroic matrix. Additional supports can be drawn from the Cu versus Pd, Pt and Ni versus Pd, Pt plots (Fig. 6) where samples of the Katpal breccia and gabbros show linear relations suggesting base-metal-sulfide controlled Pd and Pt fractionation at the later stage.

The gabbro and basalt have more fractionated PGE than the rocks of the main ultramafic unit from the Sukinda Massif. The massive chromitite, serpentinite and orthopyroxenite of the main ultramafic unit are enriched in IPGE (Ir, Os, Ru) relative to the gabbro and basalt. The Pd/

Table 3
PGM qualitative analytical data from the three chromitite samples, Sukinda Massif.

Sample No. Fig. 13	SCM/68 4 K alloy	SCM/68 1 alloy	SCM/13/80 5 alloy	SCM/13/80 4 G alloy	SCM/13/80 11 L alloy
wt %					
Os	55.0	53.8	51.4	49.6	49.3
Ir	32.8	32.4	35.5	34.9	33.6
Ru	12.3	13.9	13.2	15.5	17.0
Pt					
S					
at %					
Os	49.8	48.0	46.2	43.8	43.0
Ir	29.4	28.6	31.6	30.4	29.0
Ru	20.9	23.3	22.3	25.8	27.9
Pt					
S					

Sample No. Fig. 13	SCM/13/83 8 C alloy	SCM/13/83 12 E alloy	SCM/68 3 D alloy	SCM/13/80 12 H alloy	SCM/13/83 4 A alloy
wt %					
Os	45.6	40.8	39.8	38.2	30.9
Ir	35.3	39.3	41.6	32.5	37.0
Ru	10.8	11.7	10.1	14.5	11.8
Pt	8.3	8.2	8.6	14.9	20.3
S					
at %					
Os	41.9	37.1	36.7	34.1	28.2
Ir	32.1	35.5	38.0	28.7	33.5
Ru	18.6	20.1	17.5	24.3	20.3
Pt	7.5	7.3	7.8	13.0	18.1
S					

Sample No. Fig. 13	SCM/13/80 6 F alloy	SCM/68 2 alloy	SCM/68 5 J laurite
wt %			
Os	27.4	0.0	
Ir	37.3	31.9	9.8
Ru	14.3	68.1	55.7
Pt	21.0		
S			34.4
at %			
Os	24.6	0.0	
Ir	33.1	19.8	3.1
Ru	24.1	80.2	32.9
Pt	18.3		
S			64.0

Table 4
Comparison of compositions of the calculated parental melt from chromites with other silicate magmas from different tectonic settings (after Mondal et al., 2006; Mukherjee et al., 2012).

	$Al_2O_{3\ liquid}$ (wt%)	FeO/MgO_{liquid} (wt%)	$TiO_{2\ liquid}$ (wt%)
Sukinda Massif, Singhbhum craton (chromitite seam)	10.2–11.5	0.68–0.84	
Nuasahi Massif, Singhbhum craton (chromitite seam)	10.3–11.0	0.29–0.71	
Katpal basalt, Sukinda area (this study)	13.6	1.22-1.24	0.59-0.85
IOG high-Mg basalts, Singhbhum craton			
Sukinda area	10.7	0.94	
Nuasahi area	7.9	0.52	
Gorumahishani-Badampahar area	8.8	0.91	
Phanerozoic boninites			
Bonin island, Japan	10.6–14.4	0.7–1.4	0.10–0.52
Archean boninites			
Gadwal greenstone belt, Eastern Dharwar craton	8.78–14.10	0.48–0.96	0.24–0.36
Archean high-Mg basalts			
Barberton	12.7–13.4	0.74	0.31–0.33
Pilbara	10.1–11.7	0.58–0.75	0.39–0.43
MORB	≈15	1.2–1.6	
Oman ophiolitic chromitite	11.4–16.4	0.62 ± 0.02	0.23–0.92
Archean large layered intrusion			
Stillwater G-chromitite	12.3–12.6	1.48–1.58	
Layered Intrusions (parent magma)			
Bushveld (average 'U' type)	11.5	0.74	
Great Dyke	11.1	0.61	

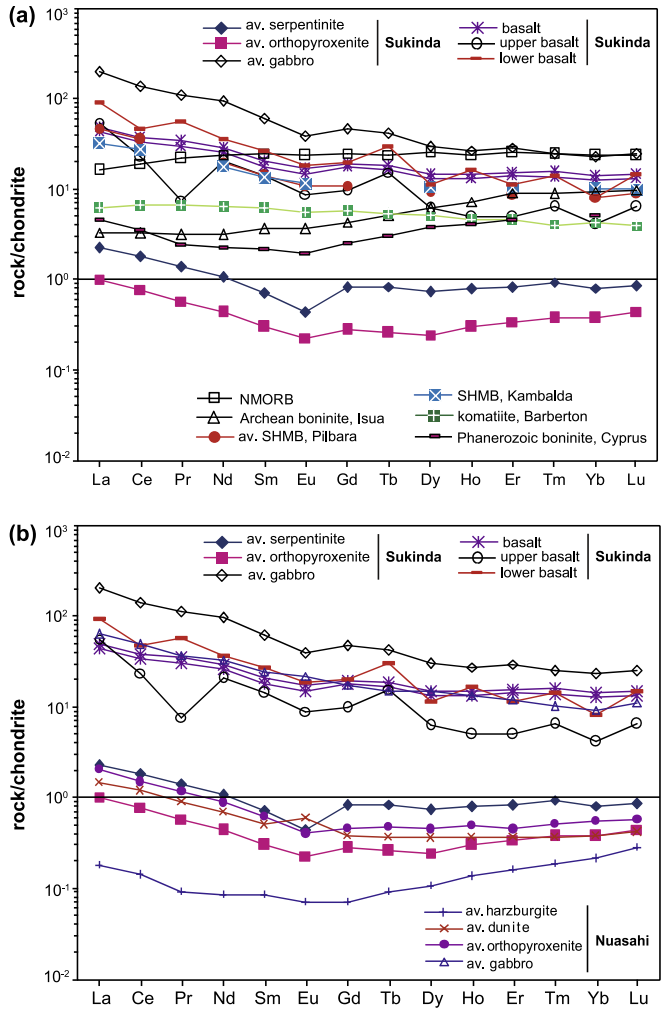

Fig. 14. Chondrite-normalized REE pattern for average serpentinite, orthopyroxenite, gabbro and basalts from the Sukinda Massif compared with (a) different types of primary magma from Archean to Phanerozoic terrains and (b) ultramafic-mafic rocks of the Nuasahi Massif. Chondrite data from McDonough and Sun (1995); upper basalt and lower basalt of Sukinda Massif from Basu et al. (1997); average harzburgite, dunite, orthopyroxenite and gabbro of the Nuasahi Massif from Mondal and Zhou (2010); average SHMB of Pilbara and Kambalda, Western Australia from Sun et al. (1989); Archean boninite (average value of 9 samples of less altered metavolcanics) of Isua from Polat et al. (2002); komatiite of Barberton (average value of 5 samples of Komati formation) from Maier et al. (2009); Phanerozoic boninite of Cyprus (sample Cyprus-9) and Phanerozoic boninite of Cape Vogel from Cameron et al. (1983).

Ir ratios in massive chromitites from Sukinda are also much lower than in serpentinites and in gabbros (Fig. 11b). Positive Ru anomalies in the ultramafic rocks of the Sukinda Massif might be due to the presence of Ru-bearing minerals (e.g., laurite) in accessory chromites within dunite and orthopyroxenite, whereas, overall IPGE enrichments in massive chromitites are due to the presence of IPGE-alloys, or micro-inclusions of IPGEs within chromite crystals (see below). Early crystallization of olivine and chromite along with high-temperature platinum-group minerals (e.g., laurite: RuS_2) or Os-Ir and Pt alloys would deplete the parental magma in Ni and IPGE and enrich it in Cu and PPGE (Pd, Pt, Rh) (Brügman et al., 1987; Puchtel and Humayun, 2000, 2001; Righter et al., 2004; Barnes and Fiorentini, 2008; Pagé et al., 2012; Prichard et al., 2017b).

The massive chromitites of the main ultramafic unit, and the chromitite fragments of the Katpal breccia contain total PGE ≈ 176–726 ppb and ≈61–279 ppb, respectively, whereas, associated ultramafic rocks (serpentinite, orthopyroxenite, peridotite)

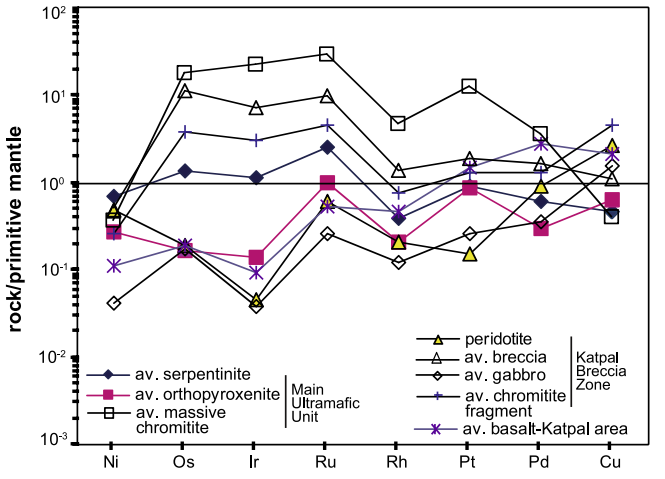

Fig. 15. Primitive mantle-normalized Ni, Cu and PGE patterns for samples (average value) of the Sukinda Massif. Primitive mantle values from Barnes et al. (1988b).

contain ≈10–71 ppb total PGE. The higher bulk-rock PGE concentration in the massive chromitites than the associated ultramafic rocks is a common observation from different tectonic settings such as layered intrusions, ophiolites, Alpine type peridotites and Alaskan type complexes (Mathez, 1999; Mondal, 2000; Ahmed and Arai, 2002; Khatun et al., 2014; Mukherjee et al., 2014). The higher bulk-rock PGE concentrations in massive chromitites are in general explained by physical presence of early-formed high-temperature PGE-bearing minerals or alloys as inclusions in chromite grains such as laurite (RuS_2) or Os-Ir alloys (Augé, 1985, 1988; Talkington and Lipin, 1986; Melcher et al., 1997; Garuti et al., 1999; Ahmed and Arai, 2003; González-Jiménez et al., 2009; Avci et al., 2017 and many others). In addition, *in situ* analysis by laser ablation-ICP-MS showed the presence of IPGE within chromite as micro-inclusions (e.g., Ballhaus and Sylvester, 2000; Locmelis et al., 2011). The SEM-EDS studies of chromites in the three massive chromitites from the main ultramafic unit of the Sukinda Massif show presence of IPGE-bearing phases as inclusions within chromite grains supporting the observed bulk rock PGE geochemical patterns of the rocks. Platinum shows a positive anomaly in some of the rocks from the Sukinda Massif (Fig. 12), which may be due to nugget effects in the powdered sample, or a natural initial heterogeneity in the magma. The serpentinite, orthopyroxenite, gabbro, basalt and some breccias from the Sukinda Massif show a negative anomaly of Ir (Fig. 12). The negative anomaly of Ir in most of the silicate rocks might be due to retention of IPGE-alloys in mantle (e.g., Orberger et al., 1998; Fonseca et al., 2012) or due to direct crystallization of IPGE-alloys at high temperature from the S-undersaturated boninitic magma (e.g., Peck and Keays, 1990; Peck et al., 1992), which entrapped within the early formed chromite grains (e.g., Finnigan et al., 2008). Experimental studies at high-temperatures by Brenan and Andrews (2001) and Andrews and Brenan (2002) also suggest that composite crystals of laurite and IPGE alloys form from a sulfur-undersaturated magma and are trapped by the growing chromite crystals.

6.3. Origin of platinum-group minerals in chromitites

The PGE mineral assemblages of the three chromitite samples representing massive chromitite bands of the main ultramafic unit from the Sukinda Massif are dominated by IPGE-bearing alloys, and mostly occurring as inclusions within chromite grains (Fig. 13; Table 3). These three samples are representing the lower two chromitite bands, **CB-1** and **CB-2** (ANNEXURE-A) and are spatially distributed. These are IPGE dominated (≈568 ppb) having higher PGE concentration (≈751 ppb) than other chromitites analyzed for present work (Table 2). Overall, the

PGE mineralogy is sulfide poor with only few grains of laurite. Arsenic-bearing PGMs are present mostly along the cracks suggesting introduction of As during hydrothermal alteration of the rocks, perhaps during serpentinization event (e.g., Bowles et al., 1994; Prichard et al., 2017a). However, IPGE-bearing alloys within primary chromites (*Cr-ratio* ranging from 0.75 to 0.81, and *Mg*-ratio from 0.62 to 0.73; Mondal et al., 2006) of the Sukinda Massif are mostly euhedral and since there is no evidence for hydrothermal alteration of these grains, suggesting their formation at an early magmatic stage (e.g., Stockman and Hlava, 1984; Talkington and Watkinson, 1986; Ahmed and Arai, 2003). Inclusions of laurite (RuS_2) grains in chromites have been found to be the most common PGE-bearing phases both in the ophiolitic and layered intrusion chromitites (e.g., Mondal and Baidya, 1997; Mondal, 2000; Mondal et al., 2001; Ahmed, 2007; Habtoor et al., 2017 and references therein). However, IPGE-alloys inclusions in chromites are mostly common in ophiolitic chromites and rare in the mafic-layered intrusions (e.g., Prichard et al., 2017b and references therein). All the IPGE-alloys in the three massive chromitites of the Sukinda Massif are Os-rich and Ru-poor like ophiolitic complexes, whereas alloys from the Alaskan-type complexes are Pt-rich. Ru-Os-Ir alloys are also common in terrestrial mantle rocks (e.g., Fonseca et al., 2012). Ahmed (2007) reported unimodal inclusions of Os-Ir-Ru alloys in chromites (*Cr*-ratio in chromite ≈ 0.8) within podiform chromitites of the late Proterozoic ophiolite from the southern Eastern Desert (SED), Egypt. In contrast, chromites (*Cr*-ratio ≈ 0.5–0.8) within podiform chromitites of same ophiolitic belt from the central Eastern Desert (CED) contain Os-rich laurite as the most dominating inclusion phase (Ahmed, 2007). According to this author the contrasting population of PGE-bearing inclusions in chromites and the compositions of host chromites from the late Proterozoic ophiolite of Egypt indicate formation of podiform chromitites in two different tectonic settings; the CED podiform chromitites were formed under a mid ocean ridge setting, whereas the SED podiform chromitites were formed in a subduction zone setting. Ahmed (2007) concluded that the variations in PGE-bearing inclusions are also indicating different temperature and fS_2 conditions in the upper mantle; the unimodal population of Os-Ir-Ru-alloys in the SED chromites indicate crystallization at relatively higher temperature in a low sulfur fugacity condition, whereas the Os-rich laurite inclusions in the CED chromites were crystallized at relatively low temperature and high sulfur fugacity conditions. Ahmed (2007) cited the experiments conducted by Brenan and Andrews (2001) and Andrews and Brenan (2002) to support these conclusions.

The Os-Ir-Ru alloys in Sukinda chromitites may begin to nucleate in mantle at high temperature and low sulfur fugacity condition, was carrying by the magma, when chromite crystallize and entrapped these IPGE-alloys (Fig. 16). Because these alloys were crystallizing and entrapped by the chromites and therefore they are high in chromitites. Augé (1988) suggested that isolated IPGE-PGMs in dunite and chromitites in the ophiolitic complexes e.g. at Vourinos and Tiébaghi ophiolitic complexes crystallized earlier than chromite in a mantle melt. These high-temperature IPGE-PGMs (and perhaps IPGE-alloys) remained suspended in the melt, where they served as sites on which new chromite grains were nucleated (e.g., Tredoux et al., 1995). Experiments by Fonseca et al. (2012) on the solubilities of Ru, Os and Ir in sulfide melts (or mattes) as a function of alloy composition at 1300 °C suggest that these IPGEs concentrate initially at the ppm level in a matte phase in the mantle. The IPGEs show low solubilities in silicate melts but have higher matte/silicate-melt partition coefficients during partial melting of the mantle. Therefore, the extraction of sulfur into silicate melt during initial melting (e.g., extraction of a MORB type magma) leads to a decrease in fS_2 that causes the exsolution of Os-Ir-Ru alloys from the refractory matte in the residual mantle peridotite. These newly formed Os-Ir-Ru alloys may stay in the mantle for long period and may be collected by a high-Mg melt like boninite that generated due to second stage melting of a MORB-depleted refractory mantle.

Production of IPGE-enriched magmas require high degree of partial melting as this facilitates the removal of refractory PGE from the mantle (e.g., Barnes et al., 1985). The primitive mineral compositions of chromite in chromitites, olivine in dunites, and orthopyroxene in orthopyroxenites from the Sukinda and Nuasahi Massifs suggest that their parental magmas were formed by high degree of mantle melting (e.g., Mondal et al., 2006). According to Mondal and co-workers (2006, 2007) chromitites and the host ultramafic rocks of the Sukinda and Nuasahi Massifs were formed from boninitic magmas generated due to the interaction of a depleted mantle with a fluid-enriched melt possibly derived in response to the dehydration of a subducting slab (Fig. 16). This would deplete the mantle further and release more refractory PGEs (or IPGE-alloys) and consequently the parental boninitic magma would be rich in IPGE that formed the PGE budget of the Sukinda chromitites. Re-Os isotopic measurements of chromites from the Nuasahi and Sukinda Massifs by Mondal et al. (2007) suggest the presence of a SCLM domain beneath the Singhbhum craton that started to form in the early Archean (~3.7 Ga) by depletion of a primitive mantle. Alternatively, the parental high-Mg magmas were derived from an early Archean depleted mantle region and this depleted region could have remained within the convecting mantle for a few hundred million years before being added to the SCLM beneath the Singhbhum craton (Mondal et al., 2007). The strong unradiogenic Os isotopic character of the chromites suggest that the parental boninitic magma was not crustally contaminated and may have been produced due to second-stage melting of a previously depleted mantle source in a supra-subduction setting (Mondal et al., 2007).

6.4. Comparison with other breccia hosted PGE deposits

In terms of geological setting and petrological character, the breccia at the Katpal area of the Sukinda Massif is similar to the breccia of the Nuasahi Massif in the Singhbhum craton. However, both PGE and base metal content of the Sukinda breccia (PGE ≈ 21.2–279.2 ppb) and the gabbroic matrix (PGE ≈ 9–12.4 ppb) is not significant like the reported PGE content in the Nuasahi breccia (258–24,100 ppb with Pd/Ir = 3–1,750; Mondal and Zhou, 2010). Compared to the Nuasahi Massif and the other breccia hosted deposits such as the Lac des Iles of Canada (e.g., Hinchey et al., 2005), the Sukinda breccia is reported to contain very little sulfide mineralization. The matrix gabbro of the Sukinda breccia is also less fractionated (and strongly PGE depleted) than the gabbroic matrix of the Nuasahi breccia as the latter is highly PGE and base-metal-sulfide enriched (Mondal and Zhou, 2010). In summary, the PGE content in the Katpal breccia of the Sukinda massif is

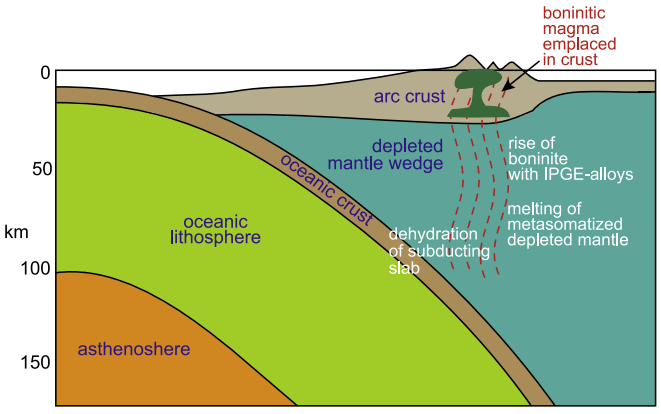

Fig. 16. Schematic representation (after Mondal et al., 2006) of possible tectonic setting for the formation of ultramafic-mafic rocks and chromitites of the Sukinda Massif. Melting of metasomatized subchondritic-refractory-mantle wedge accompanied by fluids derived from the downgoing oceanic lithospheric slab could account for the IPGE-alloys in chromites and overall IPGE-rich character of the chromitites from the Sukinda Massif.

not significant when compared to similar breccia hosted PGE-deposits within ultramafic-mafic complexes such as the similar aged Nuasahi Massif in India and the Lac des Iles in Canada. However, massive chromitites of the lower chromitite bands from the main ultramafic unit having relatively higher PGE concentrations than the other rocks in the complex require further investigations.

7. Conclusions

The relations between whole-rock major, trace and platinum-group elements indicate that the ultramafic rocks, including the chromitites of the Sukinda Massif and breccia samples, and the cementing gabbroic rocks are cogenetic. The breccia samples, including the chromitite fragments from Katpal, have higher trace element concentration than the samples of the main ultramafic unit indicating interaction with more evolved melt within the breccia zone. The ultramafic cumulates, including the chromitites, crystallized as early cumulates from a boninitic or high-Mg siliceous basaltic magma, whereas the cementing gabbro might have formed from evolved boninitic or high-Mg siliceous basaltic magma during and after the brecciation of the ultramafic rocks. The IPGE-enrichment in chromitites and positive relations of MgO with Ni, Cr and IPGEs for all rocks indicate fractionation of PGE was related to the co-crystallization of IPGE-bearing phases with the major minerals. The Zr versus Cu plot shows uniform positive relations for the ultramafic rocks, including the massive chromitites, which is interpreted to indicate that the parental boninitic magma for the ultramafic unit was S-undersaturated, however, the flat trend for the gabbros and the breccias, suggesting sulfide-saturation of the interacting evolved magma from which the matrix gabbro formed. The Sukinda breccia at Katpal is geologically and petrologically similar to the Nuasahi breccia but the former contains insignificant sulfide mineralization. Massive chromitites in the lower chromitite seams from the main ultramafic unit of the Sukinda Massif show significant PGE enrichment and warrants more investigation. The unimodal Os-Ir-Ru-alloy inclusions in chromites of these chromitites were crystallized at relatively high temperature and lower fS_2 conditions from a S-undersaturated boninitic magma. The early crystallized IPGE-alloys were trapped by the growing chromite crystals within the parental boninitic magma. Alternatively, these alloys were already present in the depleted mantle source region and collected by the boninitic parental magma generated due to second stage melting of the subchondritic mantle source region within the Singhbhum craton.

Acknowledgements

Sisir Mondal is grateful to FACOR and OMC for support and logistical help during fieldwork at Sukinda and Katpal. Sisir Mondal is thankful to NordCEE (University of Copenhagen, Denmark), CAS of Department of Geological Sciences (Jadavpur University, India) and UKIERI-UGC (Project Reference F.No.184-1/2013; project website: http://iptri.in) for field and analytical support. Sarifa Khatun is thankful to the UGC for the fellowship as a research scholar at Jadavpur University. We are thankful to Phillipe Pagé for his critical comments on an earlier version of this article which helped to improve the scientific merit of this paper. This paper is highly benefited from the critical reviews by Shoji Arai and Ahmed H. Ahmed, the two journal reviewers. We are thankful to Peter Lightfoot, Associate Editor and Franco Pirajno, Editor-in-Chief of the journal for editorial handling of this manuscript.

Appendix A. Supplementary data

Supplementary data to this article can be found online at https://doi.org/10.1016/j.oregeorev.2018.11.027.

References

Acharyya, S.K., 1993. Greenstones from Singhbhum craton, their Archean character, oceanic crustal affinity and tectonics. Proc. Nat. Acad. Sci. India 63 (A), 211–222.
Ahmed, A.H., 2007. Diversity of platinum-group minerals in podiform chromitites of the late Proterozoic ophiolite, Eastern Desert, Egypt: genetic implications. Ore Geol. Rev. 32, 1–19.
Ahmed, A.H., Arai, S., 2002. Unexpectedly high-PGE chromitite from the deeper mantle section of the northern Oman ophiolite and its tectonic implications. Contrib. Mineral. Petrol. 143, 263–278.
Ahmed, A.H., Arai, S., 2003. Platinum-group minerals in podiform chromitites of the Oman ophiolite. Can. Mineralogist 41 (3), 597–616.
Allègre, C.J., 1982. Genesis of Archean komatiites in a wet ultramafic subducted plate. In: Arndt, N.T., Nisbet, E.G. (Eds.), Komatiites. George Allen & Unwin, pp. 495–500.
Andrews, D.R.A., Brenan, J.M., 2002. Phase-equilibrium constraints on the magmatic origin of laurite + Ru–Os–Ir alloy. Can. Mineral 40, 1705–1716.
Arai, S., Miura, M., 2016. Formation and modification of chromitites in the mantle. Lithos 264, 277–295.
Augé, T., 1985. Platinum-group mineral inclusions in ophiolite chromitite from the Vourinos Complex. Greece. Can. Mineral 23, 163–171.
Augé, T., 1988. Platinum group minerals in the Tiebaghi and Vourinos ophiolitic complexes: genetic implications. Can. Mineral 26, 177–192.
Augé, T., Cocherie, A., Genna, A., Armstrong, R., Guerrot, C., Mukherjee, M.M., Patra, R.N., 2003. Age of the Baula PGE mineralization (Orissa, India) and its implications concerning the evolution of the Singhbhum Archean nucleus. Precambr. Res. 121, 85–101.
Avci, E., Uysal, I., Akmaz, R.M., Saka, S., 2017. Ophiolitic chromitites from the Kızılyüksek area of the Pozantı-Karsantı ophiolite (Adana, southern Turkey): implication for crystallization from a fractionated boninitic melt. Ore Geol. Rev. 90, 166–183.
Balaram, V., Mathur, R., Banakar, V.K., Hein, R.J., Rao, C.R.M., Rao, T.G., Dasaram, B., 2006. Determination of platinum-group of elements and gold in manganese nodule reference samples by nickel sulfide fire assay and Te-coprecipitation with ICP-MS. Indian J. Marine Sci. 35, 7–16.
Ballhaus, C., Sylvester, P., 2000. Nobel metal enrichment processes in the Merensky Reef, Bushveld Complex. J. Petrol. 41, 545–561.
Banerjee, P.K., 1972. Geology and geochemistry of the Sukinda ultramafic field, Cuttack district. Orissa. Mem. Geol. Surv. India 103, 1–158.
Barnes, S.J., Gole, M.J., Hill, R.E.T., 1988a. The Agnew nickel deposit, Western Australia: Part I. Struct. Stratigr. Econ. Geol. 83, 524–536.
Barnes, S.J., 1989. Are Bushveld U-type parent magmas boninites or contaminated komatiites? Contrib. Mineral. Petrol. 101, 447–457.
Barnes, S.J., Fiorentini, M.L., 2008. Iridium, ruthenium and rhodium in komatiites: evidence for iridium alloy saturation. Chem. Geol. 257, 44–58.
Barnes, S.-J., Naldrett, A.J., Gorton, M.P., 1985. The origin of the fractionation of platinum-group elements in terrestrial magmas. Chem. Geol. 53, 303–323.
Barnes, S.-J., Boyd, R., Korneliussen, A., Nilsson, L.P., Often, M., Pedersen, R.B., Robins, B., 1988b. The use of mantle normalization and metal ratios in discriminating between the effects of partial melting, crystal fractionation and sulphide segregation on platinum group elements, gold, nickel, and copper: example from Norway. In: Prichard, H.M., Potts, P.J., Cripp, S.J. (Eds.), Geoplatinum 87. Elsevier Appl. Scs, London, pp. 113–143.
Basu, A., Maitra, M., Roy, P.K., 1997. Petrology of mafic-ultramafic complex of Sukinda valley, Orissa. Indian Minerals 50, 271–290.
Bockrath, C., Ballhaus, C., Holzheid, A., 2004. Fractionation of the platinum group elements during mantle melting. Science 305, 1951–1953.
Bowles, J.F.W., Gize, A.P., Vaughan, D.J., Norris, S.J., 1994. Development of platinum-group minerals in laterites – initial comparison of organic and inorganic controls. Trans. Ins. Min. Met. (Sec. B, Appl. Earth Scs.) 103, 53–56.
Brenan, J.M., Andrews, D., 2001. High-temperature stability of laurite and Ru–Os–Ir alloy and their role in PGE fractionation in mafic magmas. Can. Mineral 39, 341–360.
Brügman, G.E., Arndt, N.T., Hofmann, A.W., Tobschall, H.J., 1987. Noble metal abundance in komatiite suites from Alexo, Ontario, and Gorgona Island, Colombia. Geochim. Cosmochim. Acta 51, 2159–2169.
Cameron, W.E., McCulloch, M.T., Walker, D.A., 1983. Boninite petrogenesis: chemical and Nd-Sr isotopic constraints. Earth Planet. Sci. Lett. 65, 75–89.
Chakraborty, K.L., Baidya, T.K., 1978. Geological setting and mineralogy of the chromite and some associated minerals of Kathpal, Dhenkanal district, Orissa. J. Geol. Soc. India 19, 303–309.
Chakraborty, K.L., Chakraborty, T.L., 1984. Geological features and origin of chromite deposits of Sukinda valley, Orissa. India. Miner. Deposita 19, 256–265.
Cawthorn, R.G., Davies, G., Clubley-Armstrong, A., McCarthy, T.S., 1981. Sills associated with the Bushveld Complex, South Africa: an estimate of the parental magma composition. Lithos 14, 1–15.
Crawford, A.J., Falloon, T.J., Green, D.H., 1989. Classification, petrogenesis and tectonic setting of boninites. In: Crawford, A.J. (Ed.), Boninites. Unwin Hyman, London, pp. 2–44.
Finnigan, C.S., Brenan, J.M., Mungall, J.E., McDonough, W.F., 2008. Experiments and models bearing on the role of chromite as a collector of platinum group minerals by local reduction. J. Petrol. 49, 1647–1665.
Fleet, M.E., Crocket, J.H., Stone, W.E., 1996. Partitioning of platinum-group elements (Os, Ir, Ru, Pt, Pd) and gold between sulfide liquid and basalt melt. Geochim. Cosmochim. Acta 60, 2397–2412.
Fleet, M.E., Crocket, J.H., Liu, M., Stone, W.E., 1999. Laboratory partitioning of platinum group elements (PGE) and gold with application to magmatic sulfide-PGE deposits.

Lithos 47, 127–142.
Fonseca, R.O.C., Laurenz, V., Mallmann, G., Luguet, A., Hoehne, N., Jochum, K.P., 2012. New constraints on the genesis and long-term stability of Os-rich alloys in the Earth's mantle. Geochim. Cosmochim. Acta 87, 227–242.
González-Jiménez, J.M., Gervilla, F., Proenza, J.A., Augé, T., Kerestedjian, T., 2009. Distribution of platinum-group minerals in ophiolitic chromitites. Thematic issue on 'advances in the understanding of chromitite deposits' of Applied Earth Sci. (Trans. Inst. Min. Met. B), pp. 101–110.
Garuti, G., Zaccarini, M., Economou-Eliopoulos, M., 1999. Paragenesis and composition of laurite from chromitites of Othrys (Greece): implications for Os-Ru fractionation in ophiolitic upper mantle of the Balkan Peninsula. Miner. Deposita 34, 312–319.
Grove, T.L., Parman, S.W., Dann, J.C., 1999. Conditions of magma generation for Archean komatiites from the Barberton Mountain land, South Africa. In: Fei, Y., Bertka, C.M., Mysen, B.O. (Eds.), Mantle Petrology; Field Observations and High-pressure Experimentation; A Tribute to F.R. Boyd. Geochem. Soc. Spec. Pub., pp. 155–167.
Habtoor, M.A., Ahmed, A.H., Akizawa, N., Harbi, H., Arai, S., 2017. Chemical homogeneity of high-Cr chromitites as indicator for widespread invasion of boninitic melt in mantle peridotite of Bir Tuluha ophiolite, Northern Arabian Shield. Saudi Arabia. Ore Geol. Rev. 90, 243–259.
Hicky, R.L., Frey, F.A., 1982. Geochemical characteristics of boninite series volcanics: implications for their source. Geochim. Cosmochim. Acta 46, 2099–2115.
Hinchey, J.G., Hattori, K.H., Lavigne, M.J., 2005. Geology, petrology, and controls on PGE mineralization of the southern Roby and Twilight Zones, Lac des Iles Mine, Canada. Econ. Geol. 100, 43–61.
Hofmann, A.W., 1988. Chemical differentiation of the Earth: the relationship between mantle, continental crust and oceanic crust. Earth Planet. Sci. Lett. 90, 297–314.
Keays, R.R., Lightfoot, P.C., 2010. Crustal sulfur is required to form magmatic Ni-Cu sulfide deposits: evidence from chalcophile element signatures of Siberian and Deccan Trap basalts. Miner. Deposita 45, 241–257.
Kerrich, R., Wyman, D., Fan, J., Bleeker, W., 1998. Boninite series; low Ti-tholeiite associations from the 2.7 Ga Abitibi greenstone belt. Earth Planet. Sci. Lett. 164, 303–316.
Khatun, S., Mondal, S.K., Balaram, V., Rosing, M.T., Frei, R., 2009. Geochemistry of Mesoarchean Sukinda chromite deposits (India): implications for gabbro-breccia hosted PGE mineralization. GOLDSCHMIDT 2009 (Davos). Geochim. Cosmochim. Acta. A647.
Khatun, S., Mondal, S.K., Zhou, M.-F., Balaram, V., Prichard, H.M., 2014. Platinum-group element (PGE) geochemistry of Mesoarchean ultramafic-mafic cumulate rocks and chromitites from the Nuasahi Massif, Singhbhum craton (India). Lithos 205, 322–340.
Leelananadam, C., Burke, K., Ashwal, L.D., Webb, S.J., 2006. Proterozoic mountain building in Peninsular India: an analysis based primarily on alkaline rock distribution. Geol. Magazine 143, 1–18.
Le Bas, M.J., 2000. IUGS reclassification of the high-Mg and picritic volcanic rocks. J. Petrol. 41, 1467–1470.
Lesher, C.M., Groves, D.I., 1986. Controls on the formation of komatiite-associated nickel-copper sulfide deposits. In: Friedrich, G.H. (Ed.), Geology and Metallogeny of Copper Deposits. Springer, Berlin, pp. 63–90.
Locmelis, M., Pearson, N.J., Barnes, S.J., Fioretini, M.L., 2011. Ruthenium in komatiitic chromite. Geochim. Cosmochim. Acta 75, 3645–3661.
Longhi, J., Wooden, J.L., Coppinger, K.P., 1983. The petrology high-Mg dikes from the Beartooth Mountains, Montana: a search for the parent magma of the Stillwater complex. J. Geophys. Res. Suppl. 88, B53–B69.
Majumdar, A.S., Hövelmann, J., Vollmer, C., Berndt, J., Mondal, S.K., Putnis, A., 2016a. Formation of Mg-rich olivine pseudomorphs in serpentinized dunite from the Mesoarchean Nuasahi Massif, eastern India: insights into the evolution in fluid composition at the mineral-fluid interface. J. Petrol. 57, 3–26.
Majumdar, A.S., Hövelmann, J., Mondal, S.K., Putnis, A., 2016b. The role of reacting solution and temperature on compositional evolution during harzburgite alteration: constraints from the Mesoarchean Nuasahi Massif (eastern India). Lithos 256–257, 228–242.
Mathez, E.A., 1999. On factors controlling the concentrations of platinum group elements in layered intrusions and chromitites. In: Keays, R.R., Lesher, C.M., Lightfoot, P.D., Farrow, C.E.G. (Eds.), Dynamic Processes in Magmatic Ore Deposits and their Application in Mineral Exploration. Geol. Assoc. Canada Short Cour. Notes, pp. 251–286.
Maier, W.D., Barnes, S.J., Campbell, I.H., Fiorentini, M.L., Peltonen, P., Barnes, S.-J., Smithies, R.H., 2009. Progressive mixing of meteoritic veneer into the early Earth's deep mantle. Nature 460, 620–623.
McDonough, W.F., Sun, S.-S., 1995. The composition of the Earth. Chem. Geol. 120, 223–253.
Melcher, F., Grum, W., Simon, G., Thalhammer, T.V., Stumpfl, F.E., 1997. Petrogenesis of the ophiolitic giant chromite deposits of Kempirsai, Kazakhstan: a study of solid and fluid inclusions in chromite. J. Petrol. 38, 1419–1438.
Mishra, S., Domuarari, M.P., Wiedenbeck, M., Goswami, J.N., Ray, S., Saha, A.K., 1999. $^{207}Pb/^{206}Pb$ zircon ages and the evolution of the Singhbhum Craton, eastern India: an ion microprobe study. Precambr. Res. 93, 139–151.
Mohanty, D., Sen, A.K., 2008. PGE mineralization in Katpal chromite, Sukinda ultramafic complex, Orissa. Indian Min. 42, 62–70.
Mondal, S.K., 2000. Study of chromite, sulfide and noble metal mineralization in the Precambrian Nuasahi ultramafic-mafic complex, Keonjhar district, Orissa, India. Unpublished Ph.D. thesis. Jadavpur University, Calcutta, India, pp. 193.
Mondal, S.K., 2008. Orthomagmatic Ore Deposits Related to Ultramafic-Mafic Rocks: An Introduction. In: Mondal, S.K. (Ed.), Orthomagmatic Ore Deposits Related to Ultramafic-Mafic Rocks. J. Geol. Soc. India, Sp., pp. 591–593.
Mondal, S.K., 2009. Chromite and PGE deposits of Mesoarchean ultramafic-mafic suites within the greenstone belts of the Singhbhum Craton (India): implication for mantle heterogeneity and tectonic setting. J. Geol. Soc. India 73, 1–16.
Mondal, S.K., Baidya, T.K., 1996. Stichtite [Mg_6Cr_2 $(OH)_{16}$ $CO_3.4H_2O$] in Nuasahi ultramafites, Orissa, India - its transformation at elevated temperatures. Min. Mag. 60, 836–840.
Mondal, S.K., Baidya, T.K., 1997. Platinum group mineral from the Nuasahi ultramafic-mafic complex, Orissa. India. Min. Mag. 61, 902–906.
Mondal, S.K., Zhou, M.-F., 2010. Enrichment of PGE through interaction of evolved boninitic magmas with early formed cumulates in a gabbro-breccia zone of the Mesoarchean Nuasahi Massif (eastern India). Miner. Deposita 45, 69–91.
Mondal, S.K., Baidya, T.K., Rao, K.N.G., Glascock, M.D., 2001. PGE and Ag mineralization in Breccia zone of the Precambrian Nuasahi ultramafic-mafic complex, Orissa India. Can. Mineral. 39, 979–996.
Mondal, S.K., Ripley, E.M., Li, C., Ahmed, A.H., Arai, S., Lippo, J., Stowe, C., 2003. Oxygen isotopic compositions of Cr-spinels from Archaean to Phanerozoic chromite deposits. Goldschmidt conference abstract published. Geochim. Cosmochim. Acta 18S, A301.
Mondal, S.K., Ripley, E.M., Li, C., Frei, R., 2006. The genesis of Archean chromitites from the Nuasahi and Sukinda massifs in the Singhbhum craton. India. Precambr. Res. 148, 45–66.
Mondal, S.K., Frei, R., Ripley, E.M., 2007. Os isotope systematics of Mesoarchean chromitite PGE deposits in the Singhbhum craton (India): implications for the evolution of lithospheric mantle. Chem. Geol. 244, 391–408.
Mondal, S.K., Mathez, E.A., 2007. Origin of the UG2 chromitite layer, Bushveld Complex. J. Petrol. 48, 495–510.
Mukherjee, R., Mondal, S.K., 2018. Petrogenetic evolution of chromite deposits in the Archean greenstone belts of India. In: Mondal, S.K., Griffin, W.L. (Eds.), Processes and Ore Deposits of Ultramafic-Mafic Magmas through Space and Time. Elsevier, Amsterdam, Oxford, Cambridge, pp. 159–195.
Mukherjee, R., Mondal, S.K., Rosing, M.T., Frei, R., 2010. Compositional variations in the Mesoarchean chromites of the Nuggihalli schist belt, Western Dharwar Craton (India): potential parental melts and implication for tectonic setting. Contrib. Mineral. Petrol. 160, 865–885.
Mukherjee, R., Mondal, S.K., Frei, R., Rosing, M.T., Waight, T.E., Zhong, H., Kumar, G.R.R., 2012. The 3.1 Ga Nuggihalli chromite deposits, Western Dharwar Craton (India): geochemical and isotopic constraints on mantle sources, crustal evolution and implications for supercontinent formation and ore mineralization. Lithos 155, 392–409.
Mukherjee, R., Mondal, S.K., Zhong, H., Bai, Z.-J., Balaram, V., Kumar, G.R.R., 2014. Platinum-group element geochemistry of komatiite-derived 3.1 Ga ultramafic–mafic rocks and chromitites from the Nuggihalli greenstone belt, western Dharwar craton (India). Chem. Geol. 386, 190–208.
Mukherjee, R., Mondal, S.K., González-Jiménez, J.M., Griffin, W.L., Pearson, N.J., O'Reilly, S.Y., 2015. Trace element fingerprints of chromite, magnetite and sulfide from the 3.1 Ga ultramafic-mafic rocks of the Nuggihalli greenstone belt, Western Dharwar Craton (India). Contrib. Mineral. Petrol. 169, 1–23.
Mukhopadhyay, J., Beukes, N., Armstrong, R.A., Zimmermann, U., Ghosh, G., Medda, R.A., 2008. Dating the oldest greenstone in India: a 3.51-Ga precise Pb-Pb SHRIMP zircon age for dacitic lava of the southern Iron Ore Group. Singhbhum Craton. J. Geol. 116, 449–461.
Mungall, J.E., 2014. Geochemistry of magmatic ore deposits. In: Holland, H.D., Turekian, K.K. (Eds.), Treatise on Geochemistry, 2nd ed. Elsevier, Oxford, pp. 195–218.
Mungall, J.E., Brenan, J.M., 2014. Partitioning of platinum-group elements and Au between sulfide liquid and basalt and the origins of mantle-crust fractionation of the chalcophile elements. Geochim. Cosmochim. Acta. 125, 265–289.
Orberger, B., Xu, Y., Reeves, S.J., 1998. Platinum group elements in mantle xenoliths from eastern China. Tectonophysics 296, 87–101.
Page, N.J., Banerjee, P.K., Haffty, J., 1985. Characterization of the Sukinda and Nuasahi ultramafic complex, Orissa, India by platinum group element geochemistry. Precambr. Res. 30, 27–41.
Pagé, P., Barnes, S.-J., Bedard, J.H., Zientek, M.L., 2012. *In situ* determination of Os, Ir, and Ru in chromites formed from komatiite, tholeiite and boninite magmas: implications for chromite control of Os, Ir and Ru during partial melting and crystal fractionation. Chem. Geol. 302-303, 3–15.
Pal, T., Mitra, S., 2004. P-T-fO_2 controls on a partly inverse chromite-bearing ultramafic intrusive: an evaluation from the Sukinda Massif. India. J. Asian Earth Scs. 22, 483–493.
Parman, S.W., Grove, T.L., Dann, J.C., 2001. The production of Barberton komatiites in an Archean subduction zone. Geophys. Res. Lett. 28, 2513–2516.
Parman, S.W., Grove, T.L., Dann, J.C., de Wit, M.J., 2004. A subduction origin for komatiites and cratonic lithospheric mantle. S. African J. Geol. 107, 107–118.
Peach, C.L., Mathez, E.A., 1996. Constraints on the formation of platinum group element deposits in igneous rock. Econ. Geol. 91, 439–450.
Peach, C.L., Mathez, E.A., Keays, R.R., 1990. Sulfide melt-silicate melt distribution coefficient for noble metals and other chalcophile elements as deduced from MORB: implication for partial melting. Geochim. Cosmochim. Acta 54, 3379–3389.
Peck, D.C., Keays, R.R., 1990. Geology, geochemistry, and origin of platinum-group element-chromitite occurrences in the Heazlewood River Complex. Tasmania. Econ. Geol. 85, 765–793.
Peck, D.C., Keays, R.R., Ford, R.J., 1992. Direct crystallization of refractory platinum-group element alloys from boninitic magmas: evidence from western Tasmania. Australian J. Earth Sci. 39, 373–387.
Polat, A., Hofmann, A.W., Rosing, M.T., 2002. Boninite-like volcanic rocks in the 3.7-3.8 Ga Isua greenstone belt, West Greenland: geochemical evidence for intra-oceanic subduction zone processes in the early Earth. Chem. Geol. 184, 231–254.
Prichard, H.M., Mondal, S.K., Mukherjee, R., Fisher, P.C., Giles, N., 2017a. Geochemistry and mineralogy of Pd in the magnetitite layer within the upper gabbro of the

Mesoarchean Nuasahi Massif (Orissa, India). Miner. Deposita 53, 547–564.
Prichard, H.M., Barnes, S.-J., Fisher, P.C., Paǵe, P., Zientek, M.L, 2017b. Laurite and associated PGM in the Stillwater chromitites: implications for processes of formation, and comparisons with laurite in the Bushveld and ophiolitic chromitites. Can. Mineral. 55, 121–144.
Puchtel, I., Humayun, M., 2000. Platinum group elements in Kostomuksha komatiites and basalts: implication for oceanic crust recycling and core-mantle interaction. Geochim. Cosmochim. Acta 64, 4227–4242.
Puchtel, I.S., Humayun, M., 2001. Platinum group element fractionation in a komatiitic basalt lava lake. Geochim. Cosmochim. Acta 65, 2979–2993.
Radhakrishna, B.P., Naqvi, S.M., 1986. Precambrian continental crust of India and its evolution. J. Geol. 94, 145–166.
Raju, P.V.S., Merkle, R.K.W., Gräser, P., Botha, A., Mohanty, S.K., Classen, M., 2007. Ni-Cr-PGE-minerals from the Katpal chromite mine, Sukinda chromite field, Orissa. Curr. Sci. 93, 851–854.
Righter, K., Campbell, A.J., Humayun, M., Hervig, R.L., 2004. Partioning of Ru, Rh, Pd, Re, Ir, and Au between Cr-baring spinel, olivine, pyroxene and silicate melt. Geochim. Cosmochim. Acta 68, 867–880.
Saha, A.K., 1994. Crustal evolution of Singhbhum North Orissa, Eastern India. Geol. Soc. India Mem. 27, 341.
Sarkar, N.K., Mallik, A.K., Panigrahi, D., Ghosh, S.N., 2001. A note on the occurrence of breccia zone in the Katpal chromite lode, Dhenkanal district. Orissa. Indian Min. 55, 247–250.
Sarkar, N.K., Panigrahi, D., Ghosh, S.N., Mallik, A.K., Shome, S., 2003. A note on the incidence of gold-PGM in the breccia zone of Katpal chromite quarry, Sukinda ultramafic complex, Dhenkanal district. Orissa. Indian Min. 57, 85–92.
Sattari, P., Brenan, J.M., Horn, I., McDonough, W.F., 2002. Experimental constraints on the sulphide-and chromite-silicate melt partitioning behaviour of rhenium and platinum group elements. Econ. Geol. 97, 385–398.
Sen, A.K., Mohanty, D., 2005. PGE mineralization associated with Sukinda chromite deposit, Orissa, India - an ore genetic model. In: 10th International platinum symposium, Platinum-group elements- from genesis to beneficiation and environmental impact, Oulu, Finland, August 2005, 566 - 569.
Sengupta, S., Acharya, S.K., De Smith, J.B., 1997. Geochemistry of Archean volcanic rocks from Iron Ore Supergroup, Singhbhum, eastern India. Proc. Indian Acad. Sc. (Earth Planet. Sc.) 106, 327–342.
Sharma, M., Basu, A.R., Ray, S.L., 1994. Sm-Nd isotopic and geochemical study of the Archean tonalite-amphibolite association from the eastern Indian craton. Contrib. Mineral. Petrol. 117, 45–55.
Sharpe, M.R., Hulbert, L.J., 1985. Ultramafic sills beneath the Eastern Bushveld Complex: mobilized suspensions of early Lower Zone cumulates in a parental magma with boninitic affinities. Econ. Geol. 80, 849–871.
Som, S.K., Joshi, R., 2002. Chemical weathering of serpentinite and Ni enrichment in Fe oxide at Sukinda area, Jajpur district, Orissa, India. Econ. Geol. 97, 165–172.
Stockman, H.W., Hlava, P.F., 1984. Platinum-group minerals in Alpine chromitites from southwestern Oregon. Econ. Geol. 79, 491–508.
Stowe, C.W., 1994. Composition and tectonic settings of chromite deposits through time. Econ. Geol. 89, 528–546.
Sun, S.-S., Nesbitt, R.W., McCulloch, M.T., 1989. Geochemistry and petrogenesis of Archaean and early Proterozoic siliceous high magnesian basalts. In: Crawford, A.J. (Ed.), Boninites and Related Rocks. Unwin and Hyman, London, pp. 148–173.
Talkington, R.W., Lipin, B.R., 1986. Platinum group minerals in the chromite seams of the Stillwater Complex. Montana. Econ. Geol. 81, 1179–1186.
Talkington, R.W., Watkinson, D.H., 1986. Whole rock platinum-group element trends in chromite-rich rocks in ophiolitic and stratiform igneous complexes. In: Gallagher, M.J., Ixer, R.A., Neary, C.R., Prichard, H.M. (Eds.), Metallogeny of Basic and Ultrabasic Rocks. Inst. Min. Met, London, U.K., pp. 427–440.
Tredoux, M., Lindsay, N.M., Davies, G., McDonald, L., 1995. The fractionation of platinum-group elements in magmatic system, with the suggestion of a novel causal mechanism. S. African Jour. Geol. 98, 157–167.
Wilson, A.H., Shirey, S.B., Carlson, R.W., 2003. Archaean ultradepleted komatiites formed by hydrous melting of cratonic mantle. Nature 423, 858–861.

Further reading

Barnes, S.J., 2006. Komatiites: petrology, volcanology, metamorphism, and geochemistry. Soc. Econ. Geol. Spec. Pub. 18, 13–49.